Electronic Supplementary Material (ESI) for RSC Applied Interfaces.

Supplemental Information:

Lithium-Ion Battery Functionality over Broad Operating Conditions via Local High Concentration Fluorinated Ester Electrolytes

Calvin D. Quilty[1,2]; Edelmy J. Marin Bernardez[1,2]; Andrew Nicoll[1,2]; Md Jamil Hossain[3], Arun Kingan[1,2]; David J. Arnot[2,4]; Hafsa A. Mohamed[5,6]; Ciara L. O'Connor[5,7]; Xiao Tong[8]; Cherno Jaye[9]; Daniel A. Fischer[9]; Lei Wang[2,10]; Yue Qi[3], Esther S. Takeuchi[1,2,4,10]; Amy C. Marschilok[1,2,4,10]; Shan Yan[2, 10]; David C. Bock[2,10*]; Kenneth J. Takeuchi[1,2,4,10*]

1. Department of Chemistry, Stony Brook University, Stony Brook, NY, 11794, United States of America.
2. Institute of Energy: Sustainability, Environment, and Equity (I:SEE), Stony Brook University, Stony Brook, NY, 11794, United States of America.
3. School of Engineering, Brown University, Providence, RI, 02912, United States of America.
4. Department of Materials Science and Chemical Engineering, Stony Brook University, Stony Brook, NY, 11794, United States of America.
5. Science Undergraduate Laboratory Internship (SULI) Program, Brookhaven National Laboratory, Upton, NY, 11973, United States of America.
6. Department of Chemistry, University of Rochester, Rochester, NY 14627, United States of America.
7. Department of Chemistry, The College of Wooster, Wooster, OH 44691, United States of America.
8. Center for Functional Nanomaterials, Brookhaven National Laboratory, Upton, NY, 11973, United States of America.
9. Material Measurement Laboratory, National Institute of Standards and Technology, Gaithersburg, Maryland 20899, United States of America.
10. Interdisciplinary Science Department, Brookhaven National Laboratory, Upton, NY, 11973, United States of America.

*corresponding authors: DCB, dbock@bnl.gov; KJT, kenneth.takeuchi.1@stonybrook.edu

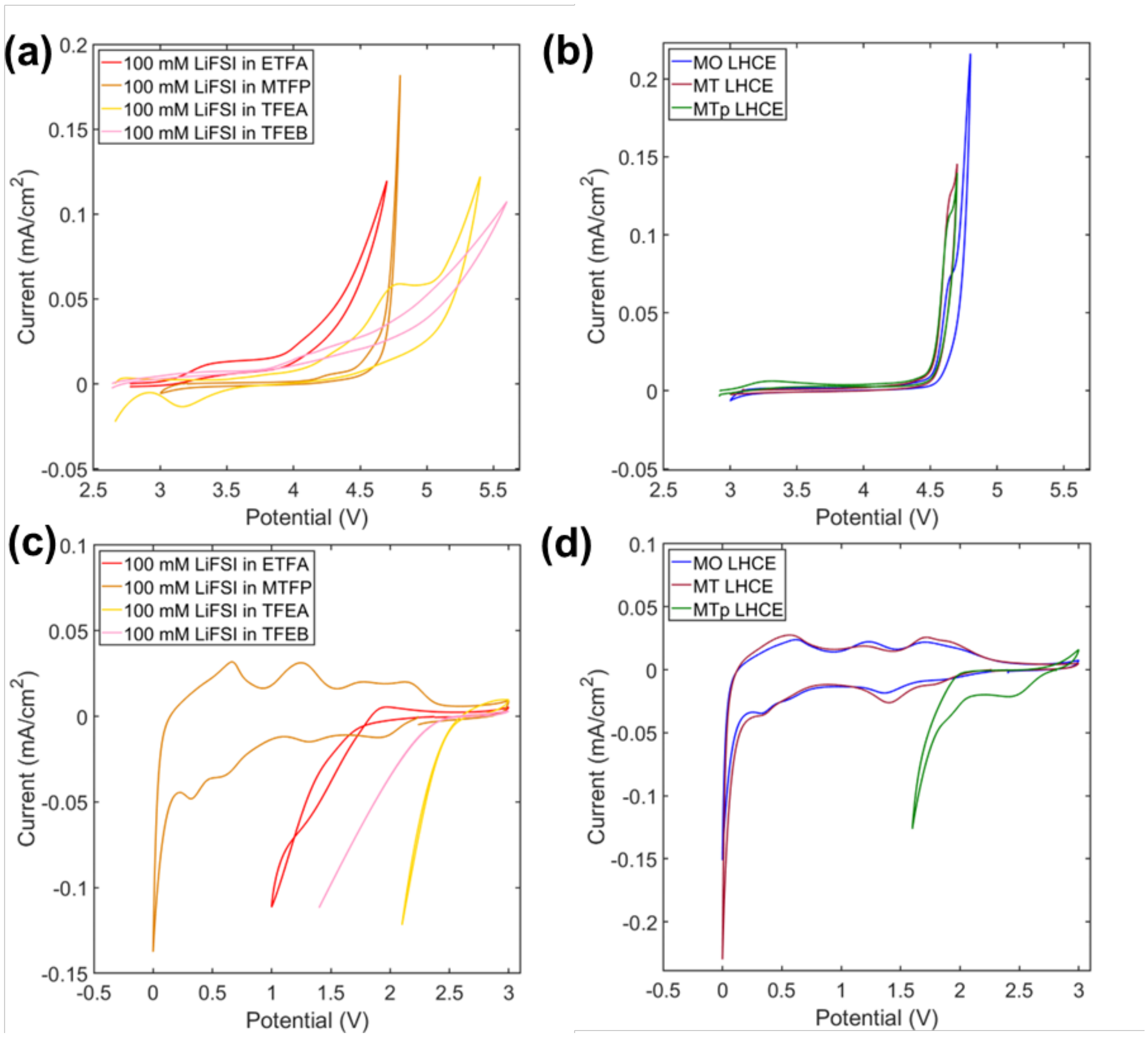

Figure S1. Voltage stability of solvents and diluents. (a) and (c) upper voltage stability and lower voltage stability of ethyl trifluoroacetate (ETFA), methyl 3,3,3-trifluoropropionate (MTFP), 2,2,2-trifluoroethylacetate (TFEA), and 2,2,2-trifluoroethylbutyrate (TFEB). (b) and (d) upper voltage stability and lower voltage stability of 2.25 M LiFSI in MTFP with 2,2,3,3-tetrafluoropropyl trifluoroacetate (MTp LHCE), 2,2,2-trifluoroethyl 1,1,2,2-tetrafluoroethylether (MT LHCE), or 1H,1H, 5H-Octafluoropentyl 1,1,2,2-tetrafluoroethylether (MO LHCE) in a 2:1 molar ratio.

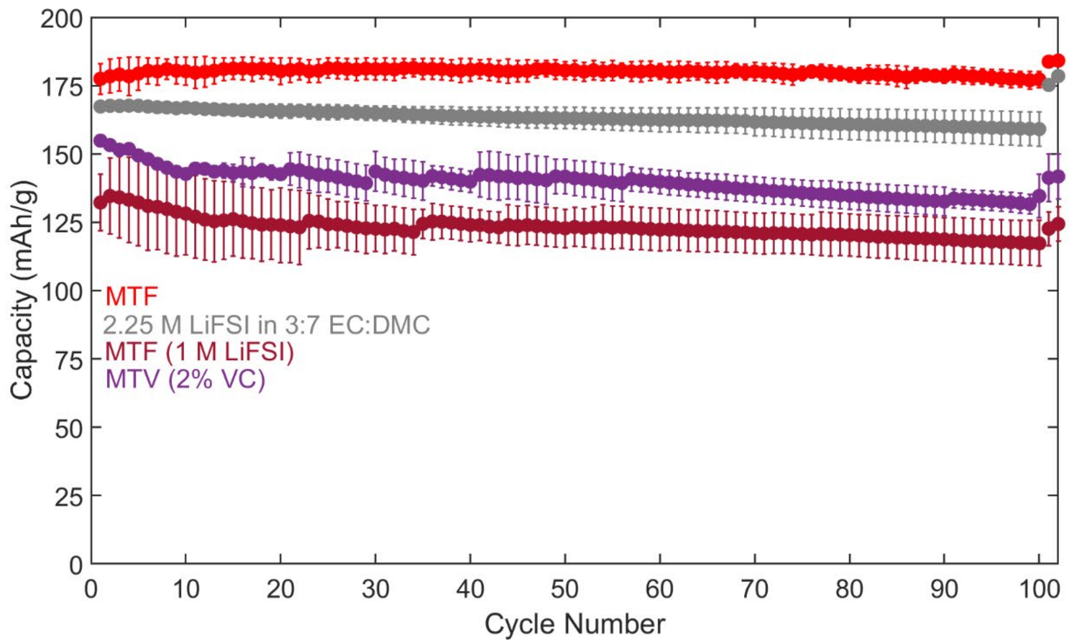

Figure S2. Discharge capacities *vs*. cycle number for cells cycled under the 1C/1C CCCV condition with MTF, 2.25 M LiFSI EC:DMC, MTF (1 M LiFSI), and MTV (2% VC) electrolytes.

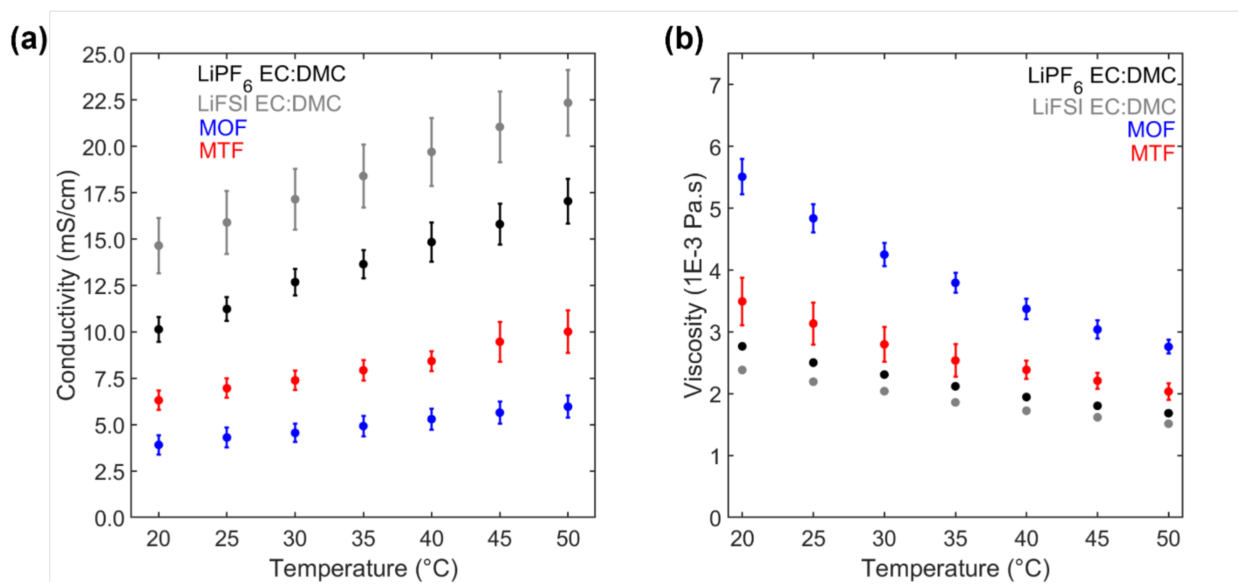

Figure S3. Properties of the LHCE electrolytes [(2.25 mol/L LiFSI in MTFP):OFPTFE 2:1]:FEC 9:1 (MOF) and [(2.25 mol/L LiFSI in MTFP):TFETFE 2:1]:FEC 9:1 (MTF) compared with control formulations (1 mol/L $LiPF_6$ in 3:7 EC:DMC and 1 mol/L LiFSI in 3:7 EC:DMC). Plots of (a) conductivity and (b) viscosity.

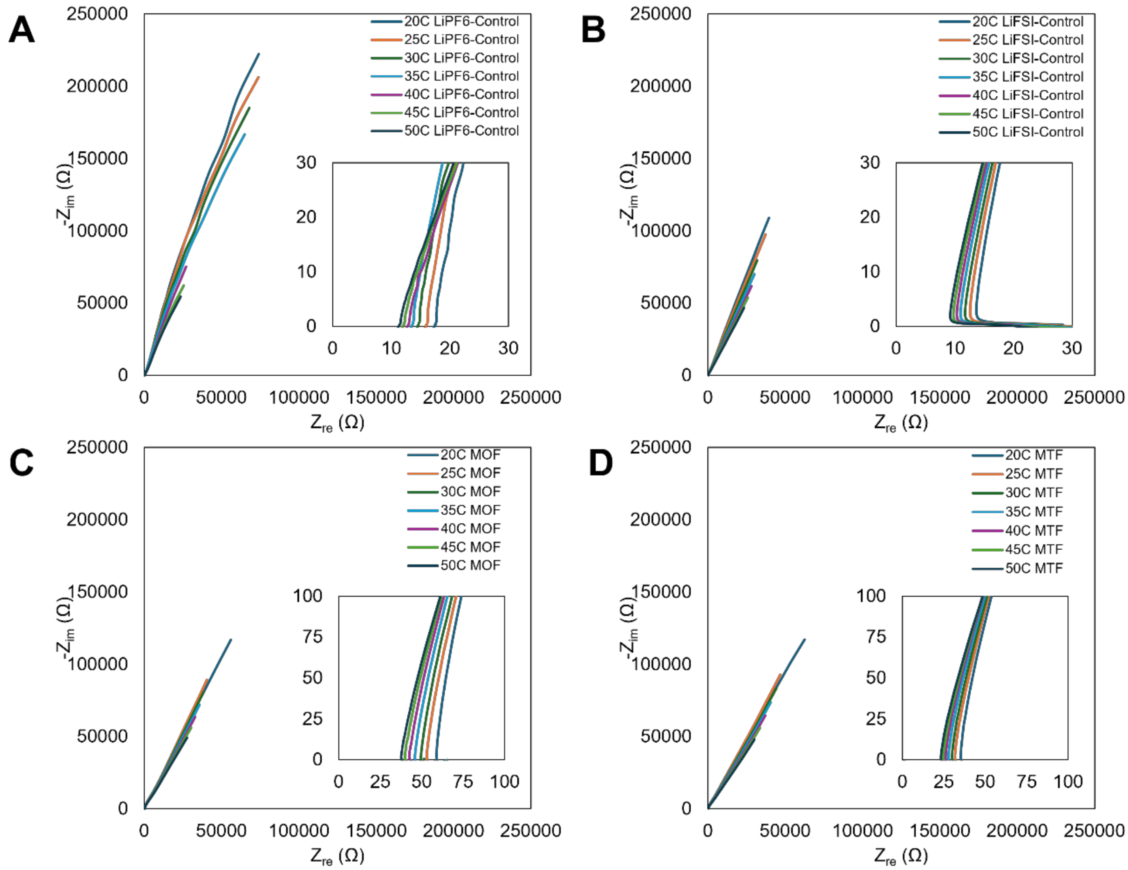

Figure S4. Representative Nyquist plots of impedance used for conductivity measurements of (A) $LiPF_6$ control, (B) LiFSI Control, (C) MOF, and (D) MTF.

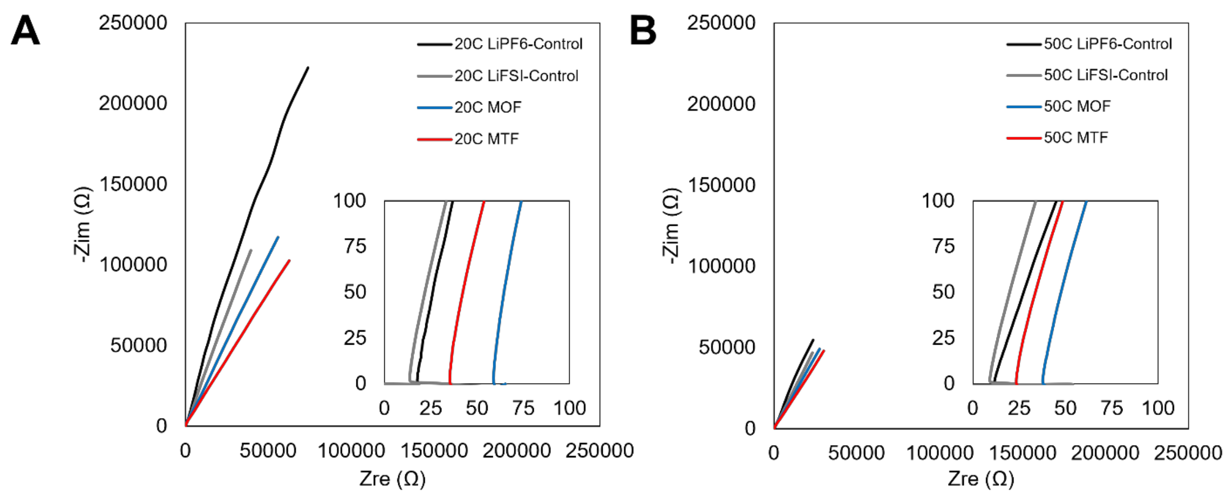

Figure S5. Selected representative Nyquist plots of impedance for conductivity measurements at (A) 20 °C and (B) 50 °C.

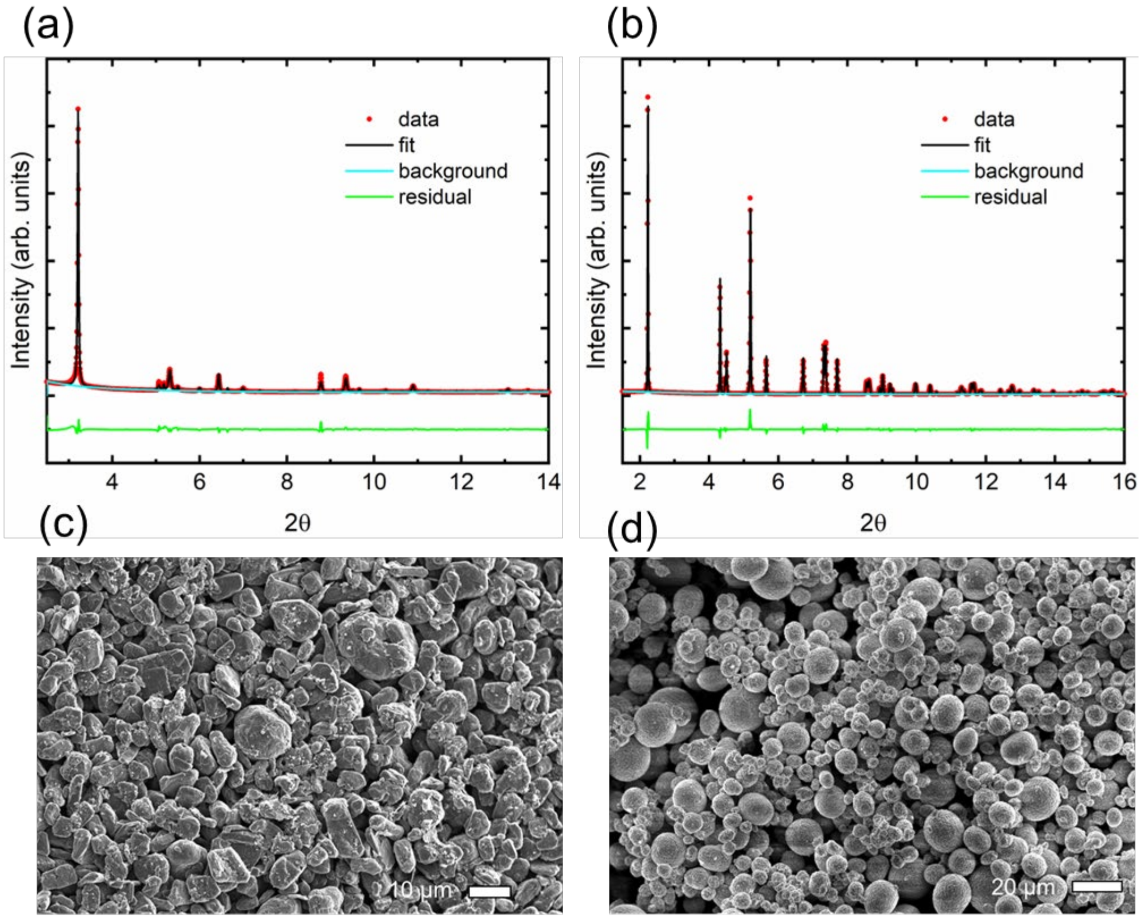

Figure S6. (a,b) Rietveld refinements of XRD patterns and (c, d) SEM images of (a, c) graphite and (b, d) NMC811 active materials. Refinement of the natural graphite was done with both hexagonal (space group $P6_3/mmc$) and rhombohedral (space group $R\overline{3}m$) phases with weight fractions of 77 % and 23 % respectively. The NMC811 was fit with the $R\overline{3}m$ structure with no detectable impurities and was determined to have crystallite size of > 180 nm and low microstrain (< 0.3 %). SEM characterization indicated that both materials have spherical particle morphologies with similar average size of 6.8 ± 2.5 µm and 10.0 ± 3.9 µm for graphite and NMC811, respectively.

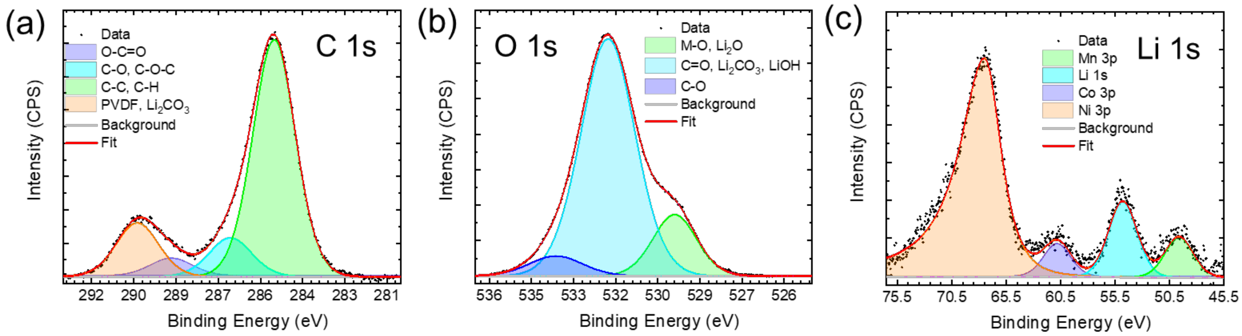

Figure S7. XPS of pristine $LiNi_{0.8}Mn_{0.1}Co_{0.1}O_2$. (a) C1s, (b) O 1s, (c) Li 1s regions. Examination of the C1s spectra reveal adventitious carbon peaks at ≈285eV as well as oxygenated adventitious carbon species at ≈ 286 eV and ≈ 288 eV, consistent with previous reports of pristine NMC materials.[1, 2] Additionally there is a peak at ≈ 289 eV indicating the presence of Li_2CO_3 in the pristine material.[3-5] The O 1s spectra show a large corresponding peak at ≈ 531.5 eV for the carbonate bonding moiety; contributions from LiOH are also possible at this binding energy.[6] Peaks are also observed at 534 eV corresponding to C-O bonds and at ≈ 529 eV, assigned to metal to oxygen bonding associated with the NMC lattice[7] as well as possibly Li_2O which occurs at the similar binding energy.[8] Examination of the Li 1s spectra reveals a peak at ≈ 54 eV which may correspond to Li in the cathode structure, Li_2CO_3, LiOH, or Li_2O which are reported to have overlapping binding energies.[9, 10]

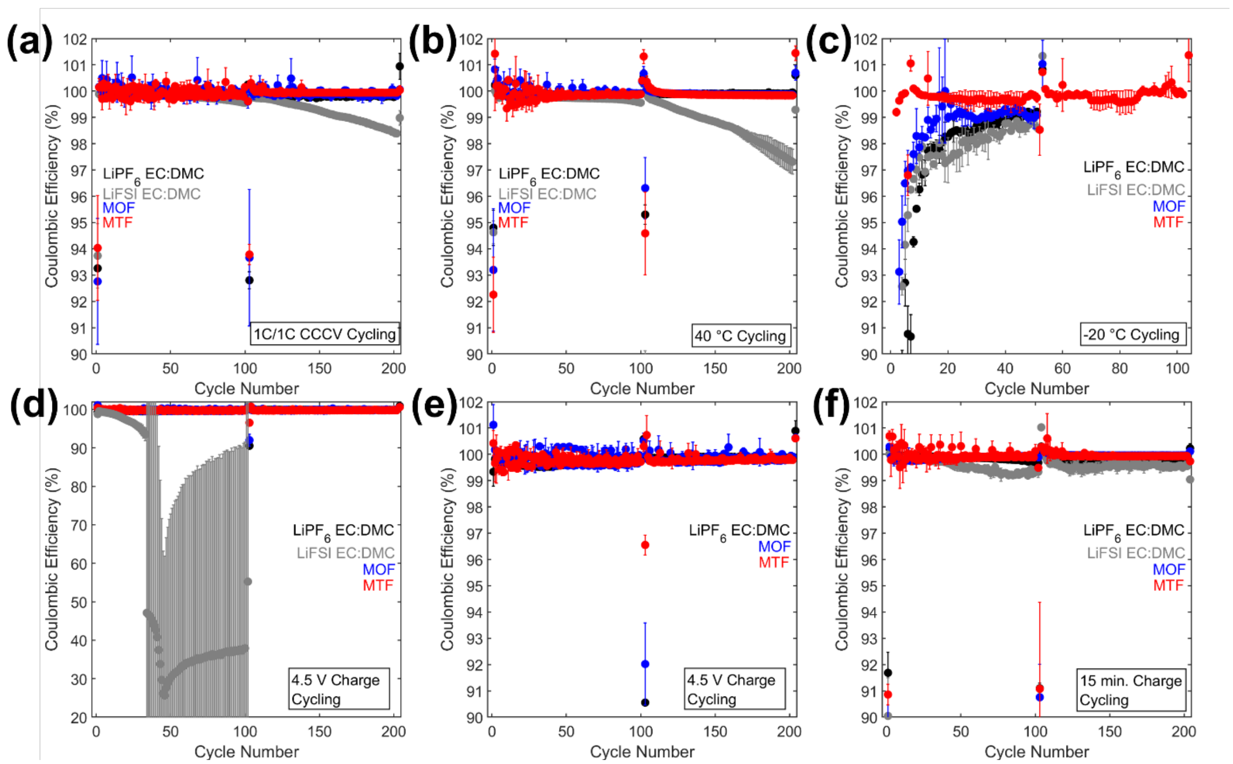

Figure S8. Coulombic efficiency *vs*. cycle number for the (a) 1C/1C CCCV, (b) 40 °C, (c) -20 °C, (d and e) 4.5 V charge, and (f) 15 min charge condition.

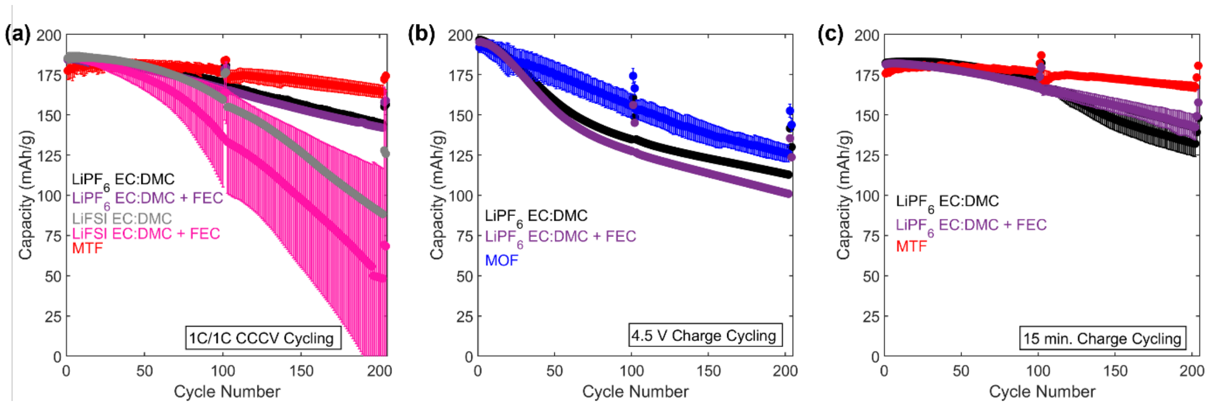

Figure S9. Discharge capacities *vs*. cycle number for the (a) 1C/1C CCCV, (b) 4.5 V charge, and (c) 15 min charge condition for cells with $LiPF_6$ EC:DMC, $LiPF_6$ EC:DMC + 10% FEC, LiFSI EC:DMC, LiFSI EC:DMC + 10% FEC, and MOF/MTF electrolytes.

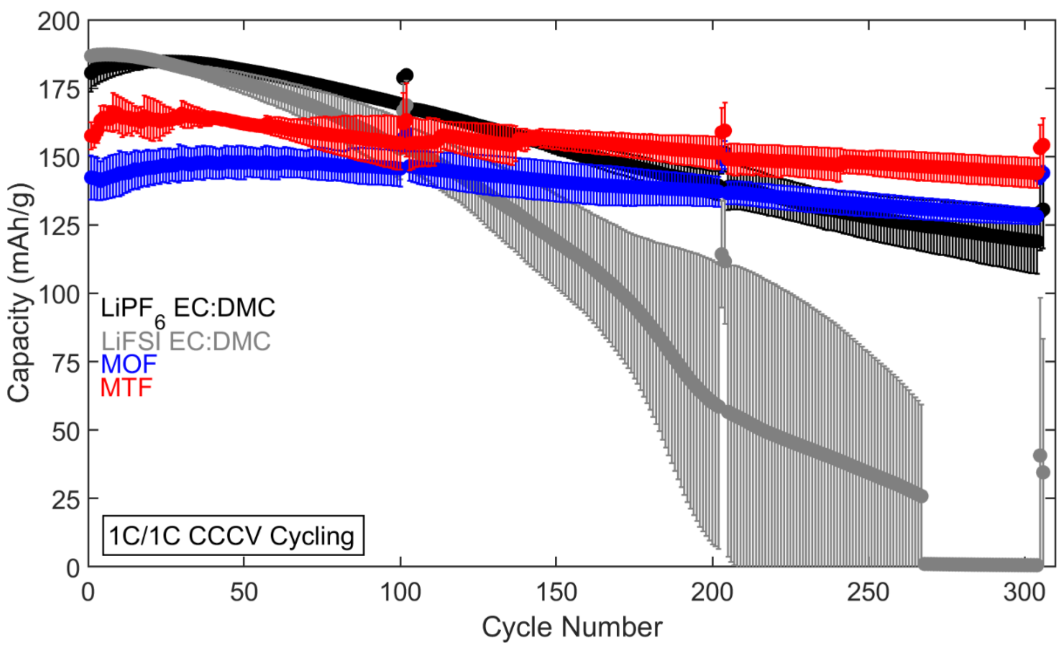

Figure S10. Discharge capacities *vs*. cycle number for cells with 3.0 mAh/cm^2 cathodes cycled under the 1C/1C CCCV condition with $LiPF_6$ EC:DMC, LiFSI EC:DMC, MOF, and MTF electrolytes.

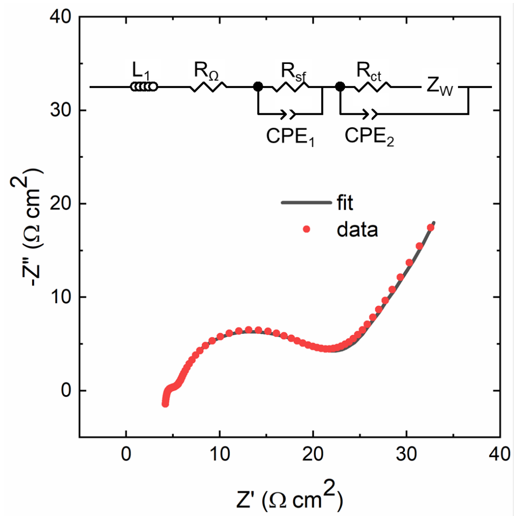

Figure S11. Equivalent circuit model used to fit impedance data with example fit. The equivalent circuit uses two RQ elements in series to model the semicircular features in the Nyquist plots. The first resistor (R_{Ω}) represents Ohmic resistances of the cell components while R_{sf} and CPE_1 are used to fit the high frequency semicircular feature, corresponding to the ionic resistances and capacitances of the interphase films at the electrodes. The third resistor (R_{ct}), second constant phase element (CPE_2), and Warburg element (Z_w) were used to fit the spectral middle to low frequency range and approximate the charge transfer resistance, double layer capacitance, and solid state diffusion of Li^+ ions in the electrodes, respectively.[11-15]

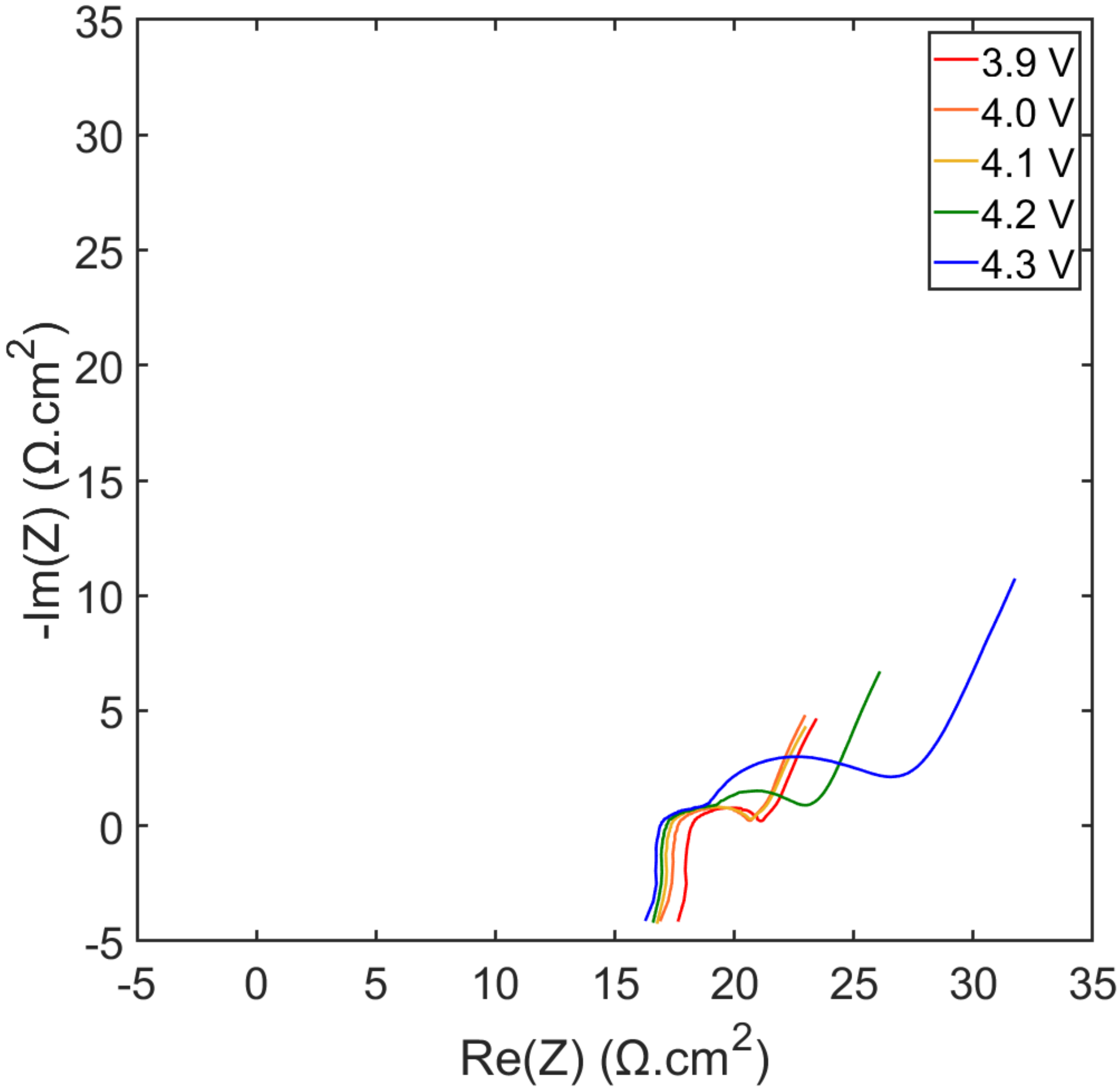

Figure S12. EIS on a post-formation cell with $LiPF_6$ EC:DMC electrolyte. The cell was charged to 3.9 V, 4.0 V, 4.1 V, 4.2 V, and 4.3 V at C/10 and EIS was collected at each voltage.

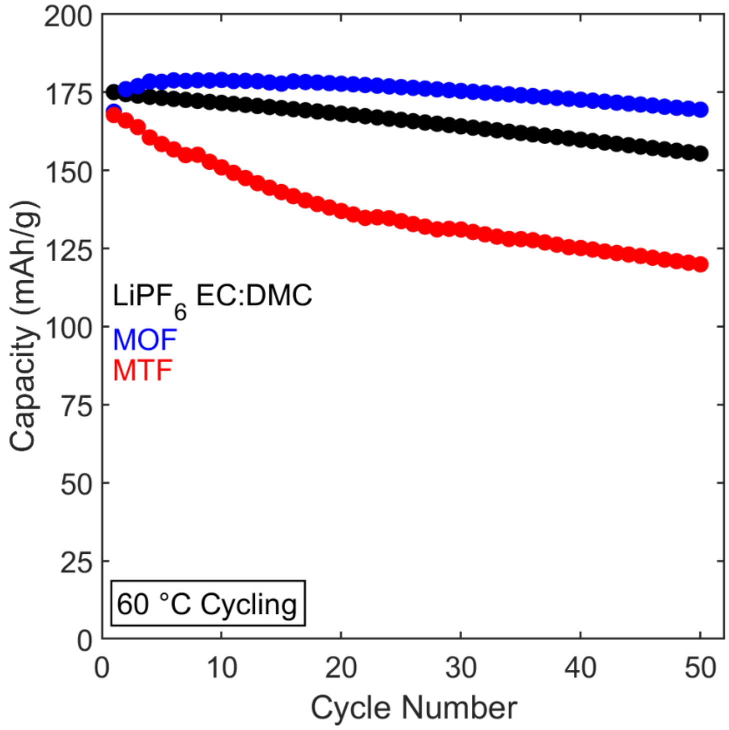

Figure S13. Discharge capacities *vs*. cycle number for cells cycled at 60 °C with $LiPF_6$ EC:DMC, MOF, and MTF electrolytes.

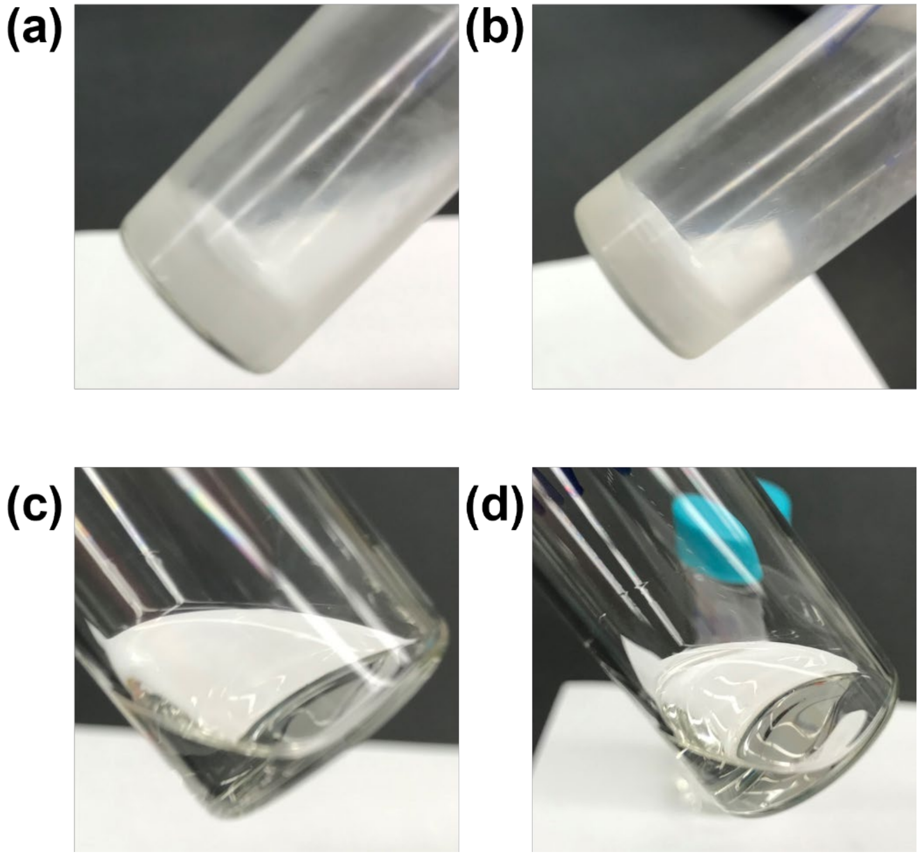

Figure S14. Images of electrolytes after being stored at -20 °C for 48 hours. (a) $LiPF_6$ EC:DMC, (b) LiFSI EC:DMC, (c) MOF, and (d) MTF.

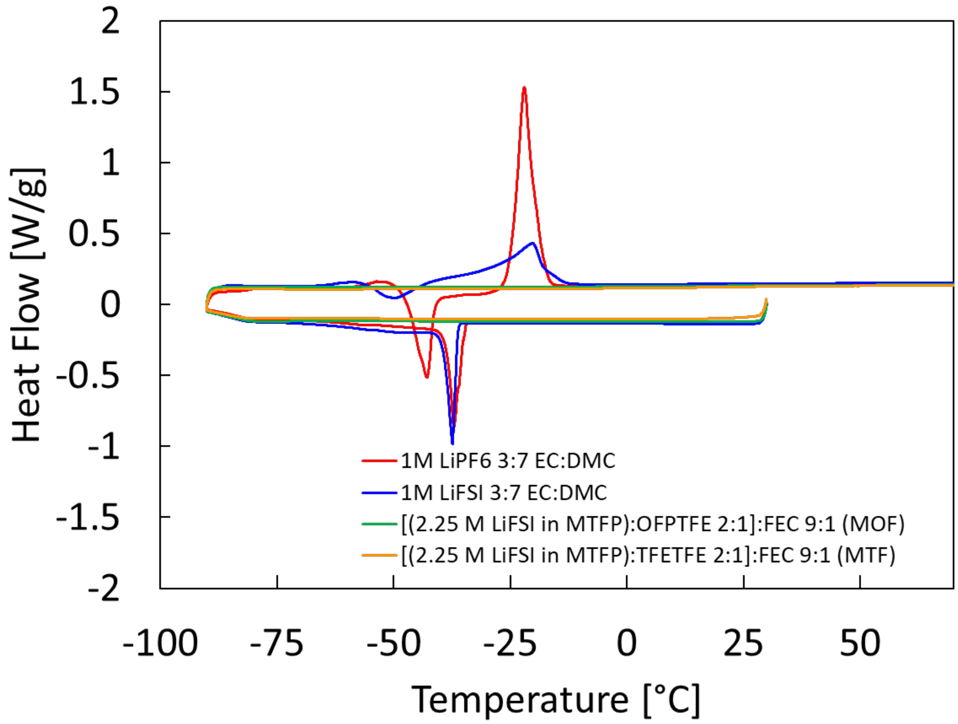

Figure S15. Differential Scanning Calorimetry (DSC) measurements of the LHCE electrolytes [(2.25 mol/L LiFSI in MTFP):OFPTFE 2:1]:FEC 9:1 (MOF) and [(2.25 mol/L LiFSI in MTFP):TFETFE 2:1]:FEC 9:1 (MTF) compared with control formulations (1 mol/L $LiPF_6$ in 3:7 EC:DMC and 1 mol/L LiFSI in 3:7 EC:DMC).

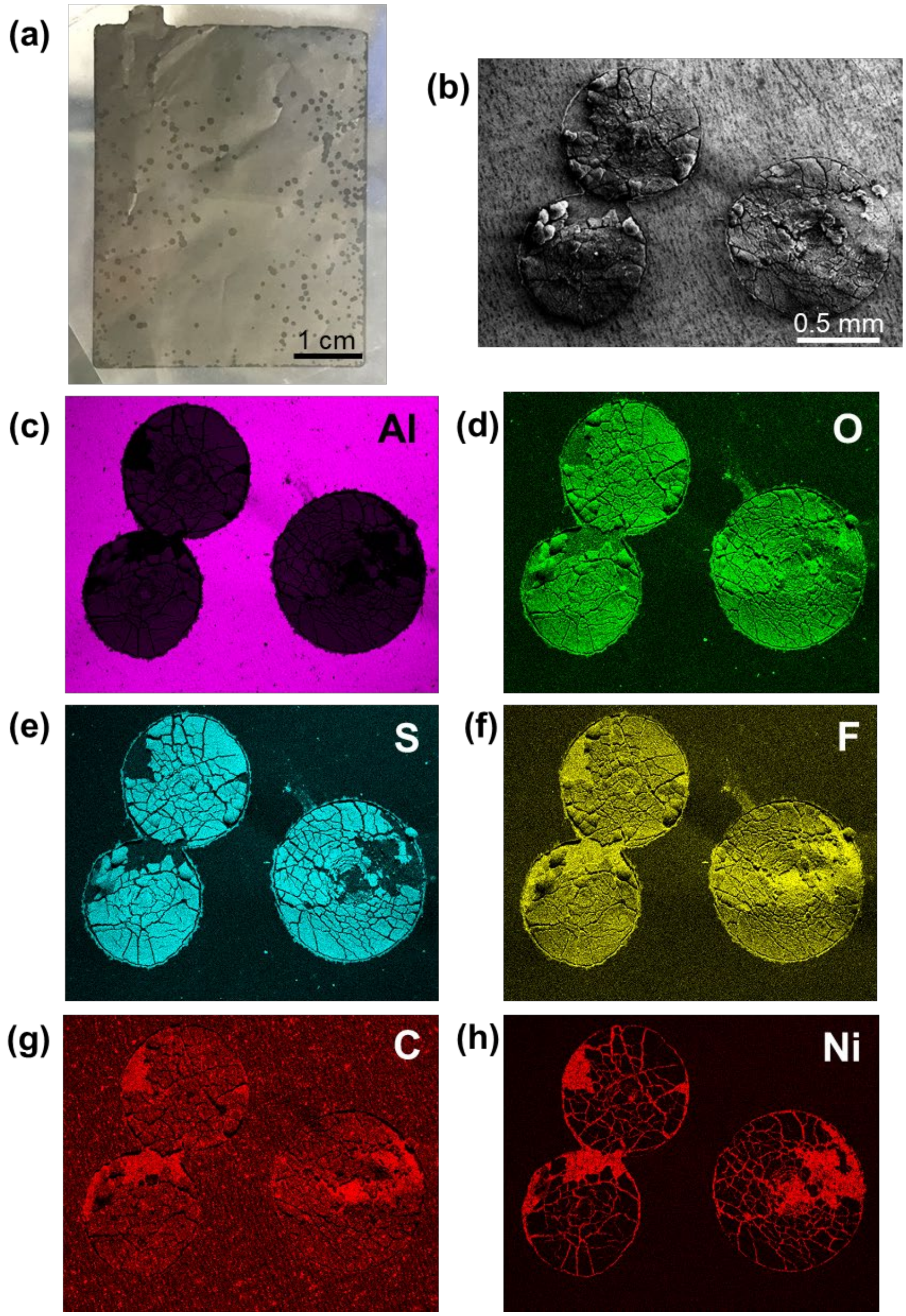

Figure S16. (a) Image of corrosion of a cathode current collector cycled in LiFSI EC:DMC under the high voltage cycling condition. (b) Secondary electron SEM image of three of the corroded regions in (a). (c-h) EDS maps of (b). (c) Al, (d) O, (e) S, (f) F, (g) C, and (h) Ni.

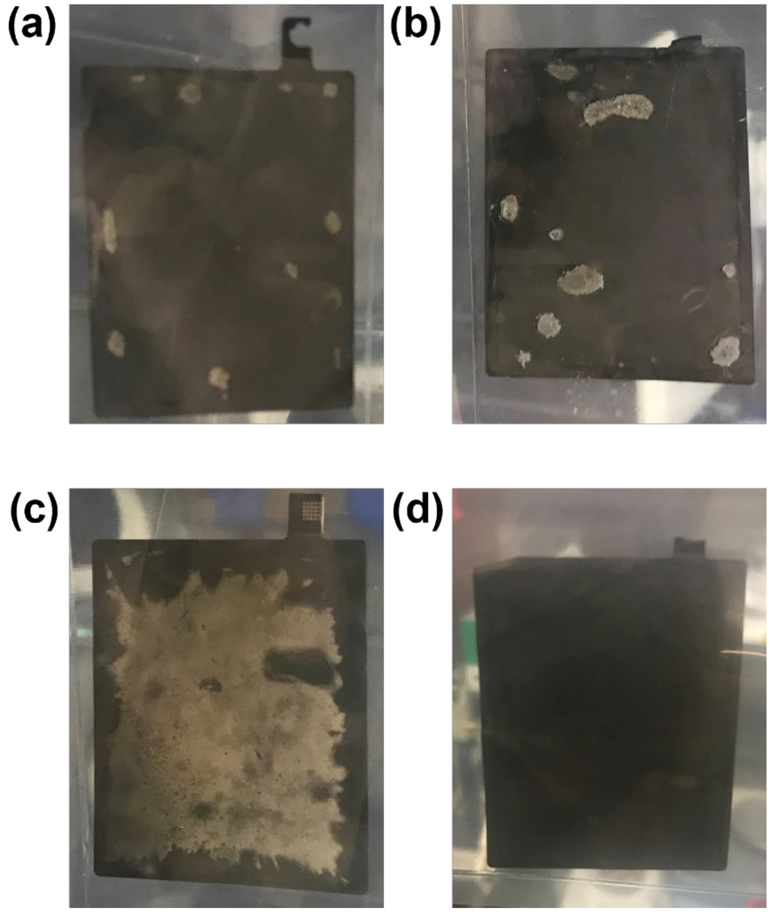

Figure S17. Optical images of (a) $LiPF_6$ EC:DMC, (b) LiFSI EC:DMC, (c) MOF, and (d) MTF anodes after fast charge cycling, showing dramatic reduction in Li plating on the MTF cycled anode.

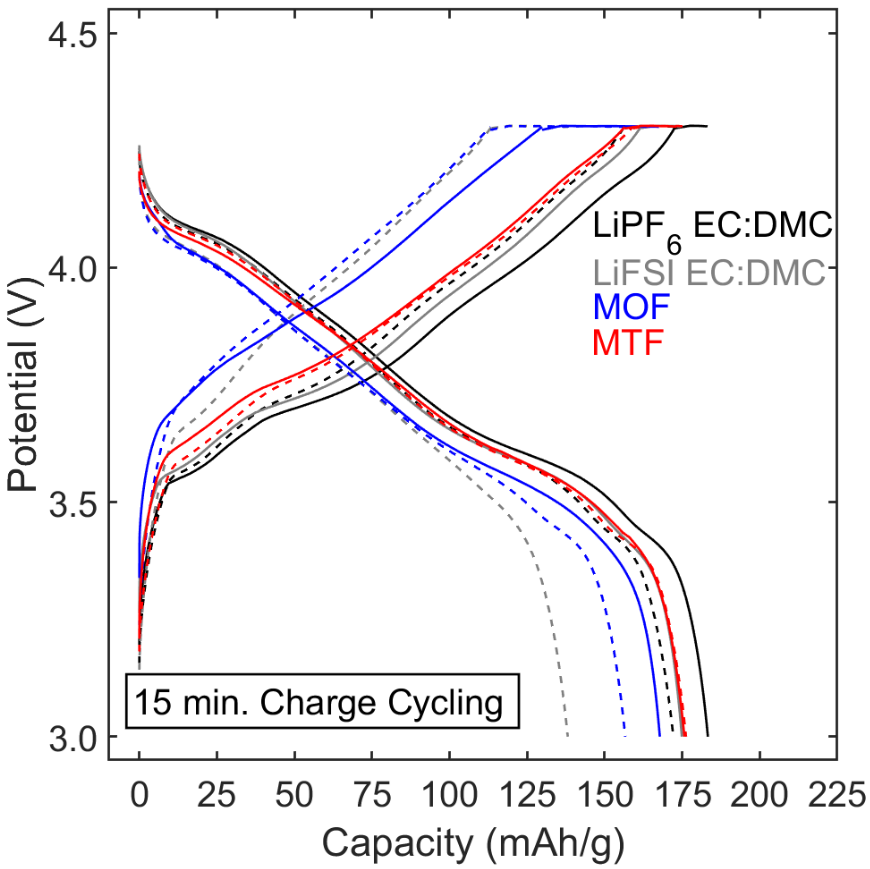

Figure S18. Voltage profiles during cycle 1 (solid lines) and cycle 100 (dashed) lines for cells cycled under the 15 min charging condition.

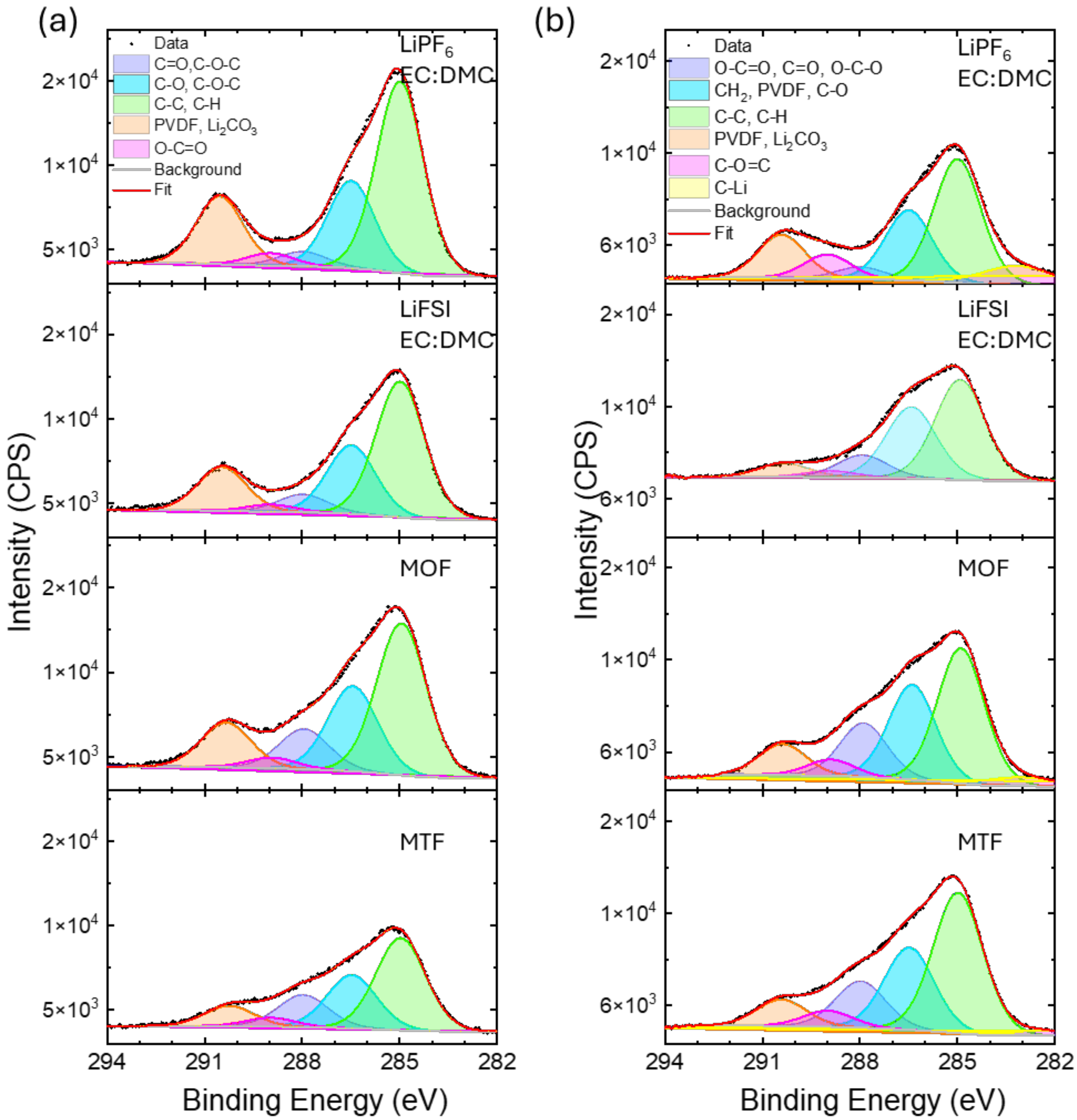

Figure S19. XPS C 1s spectra of recovered (a) NMC811 cathodes and (b) graphite anodes after 200x cycles under the 1C/1C CCCV cycling condition with either $LiPF_6$ EC:DMC, LiFSI EC:DMC, MOF, or MTF electrolytes.

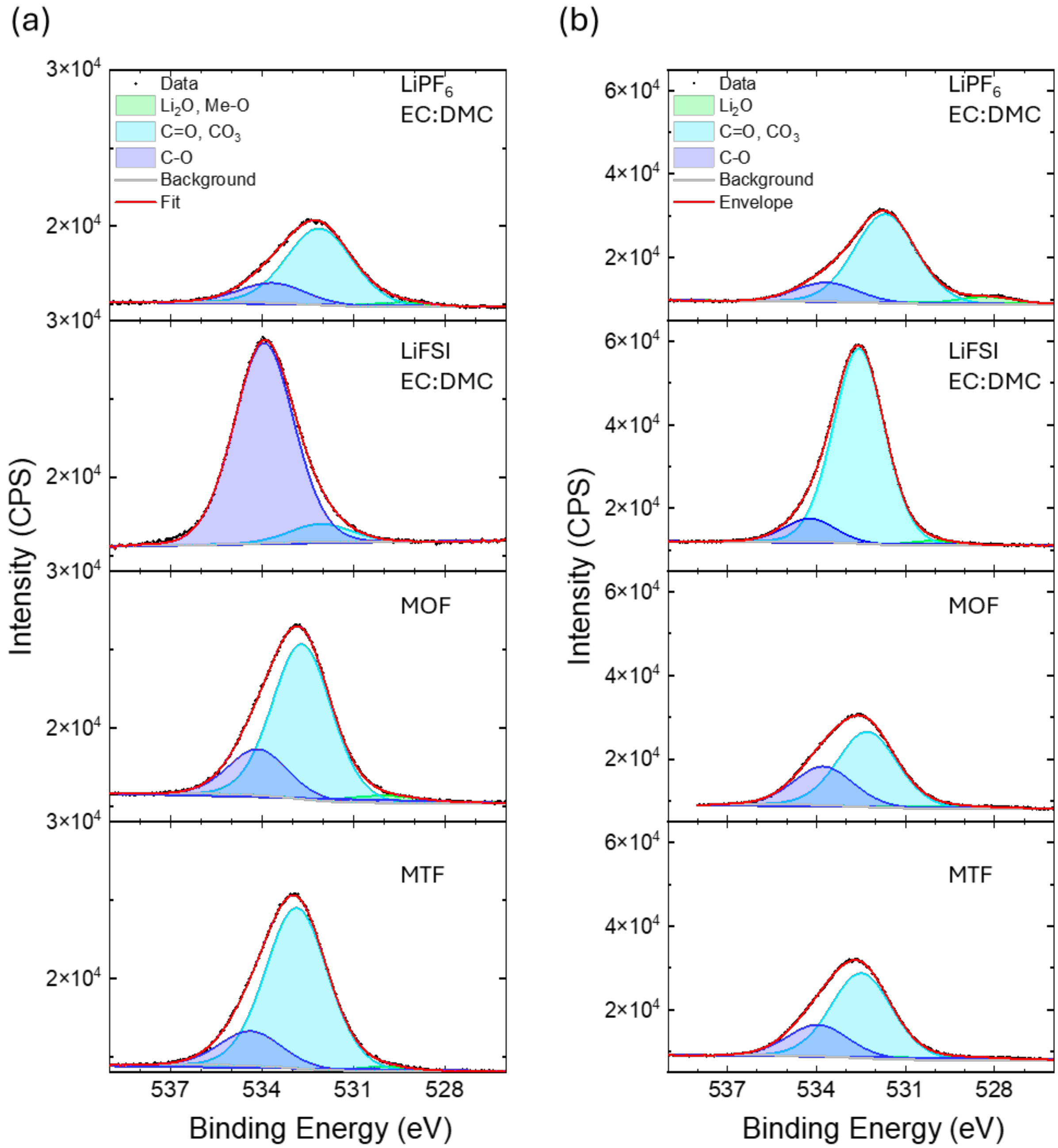

Figure S20. XPS O 1s spectra of recovered (a) NMC811 cathodes and (b) graphite anodes after 200x cycles under the 1C/1C CCCV cycling condition with either $LiPF_6$ EC:DMC, LiFSI EC:DMC, MOF, or MTF electrolytes.

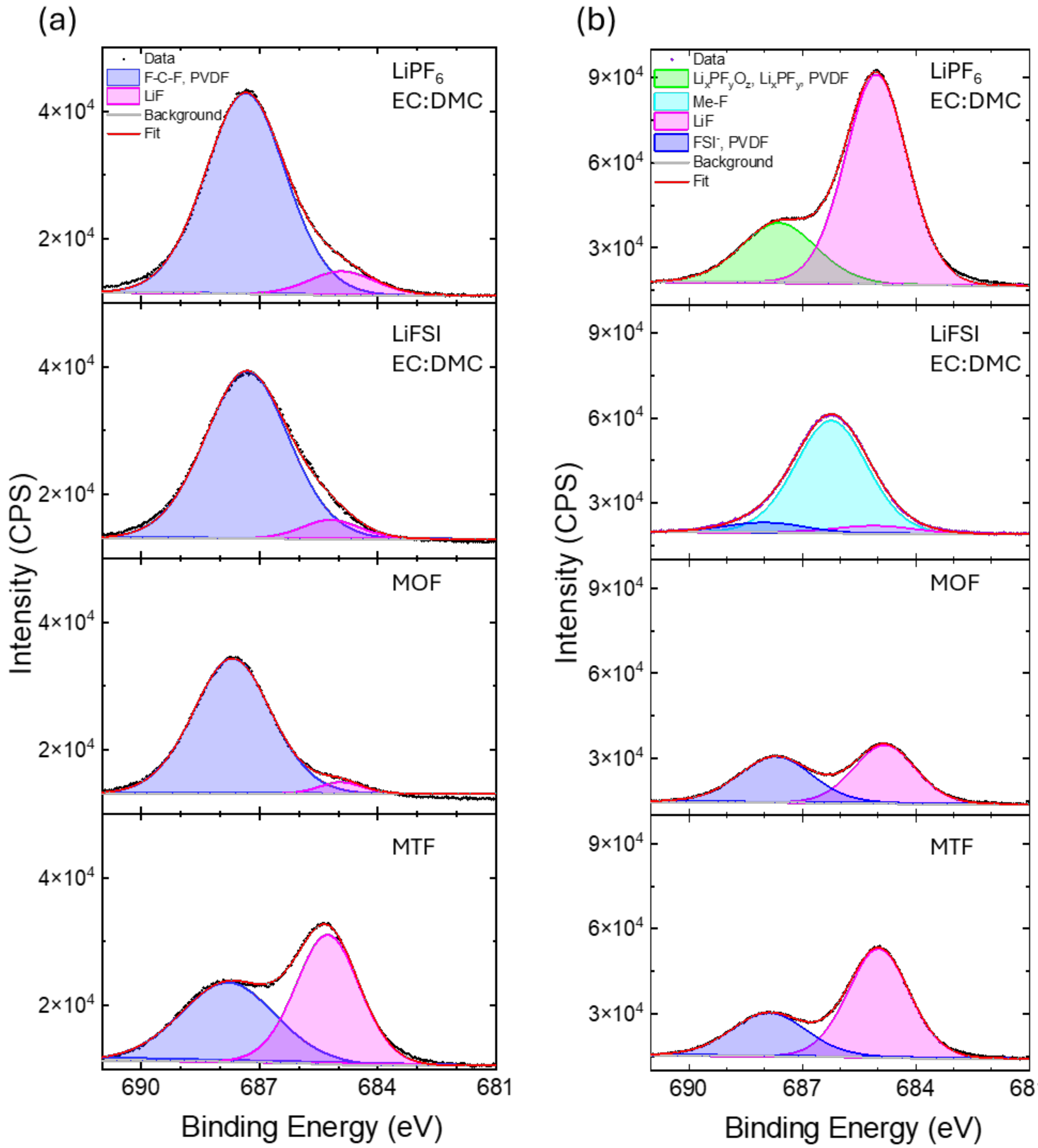

Figure S21. XPS F 1s spectra of recovered (a) NMC811 cathodes and (b) graphite anodes after 200x cycles under the 1C/1C CCCV cycling condition with either $LiPF_6$ EC:DMC, LiFSI EC:DMC, MOF, or MTF electrolytes.

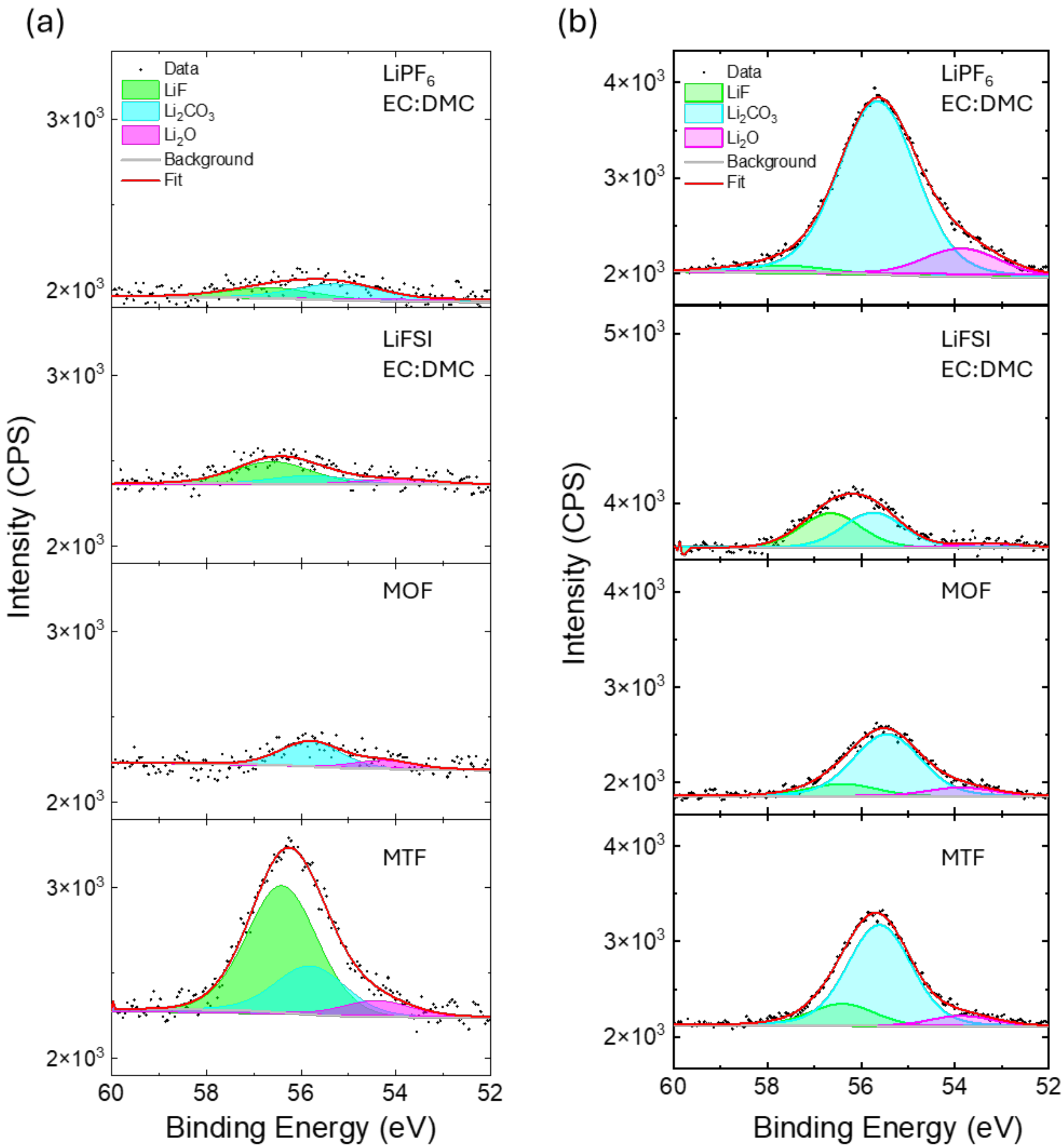

Figure S22. XPS Li 1s spectra of recovered (a) NMC811 cathodes and (b) graphite anodes after 200x cycles under the 1C/1C CCCV cycling condition with either $LiPF_6$ EC:DMC, LiFSI EC:DMC, MOF, or MTF electrolytes.

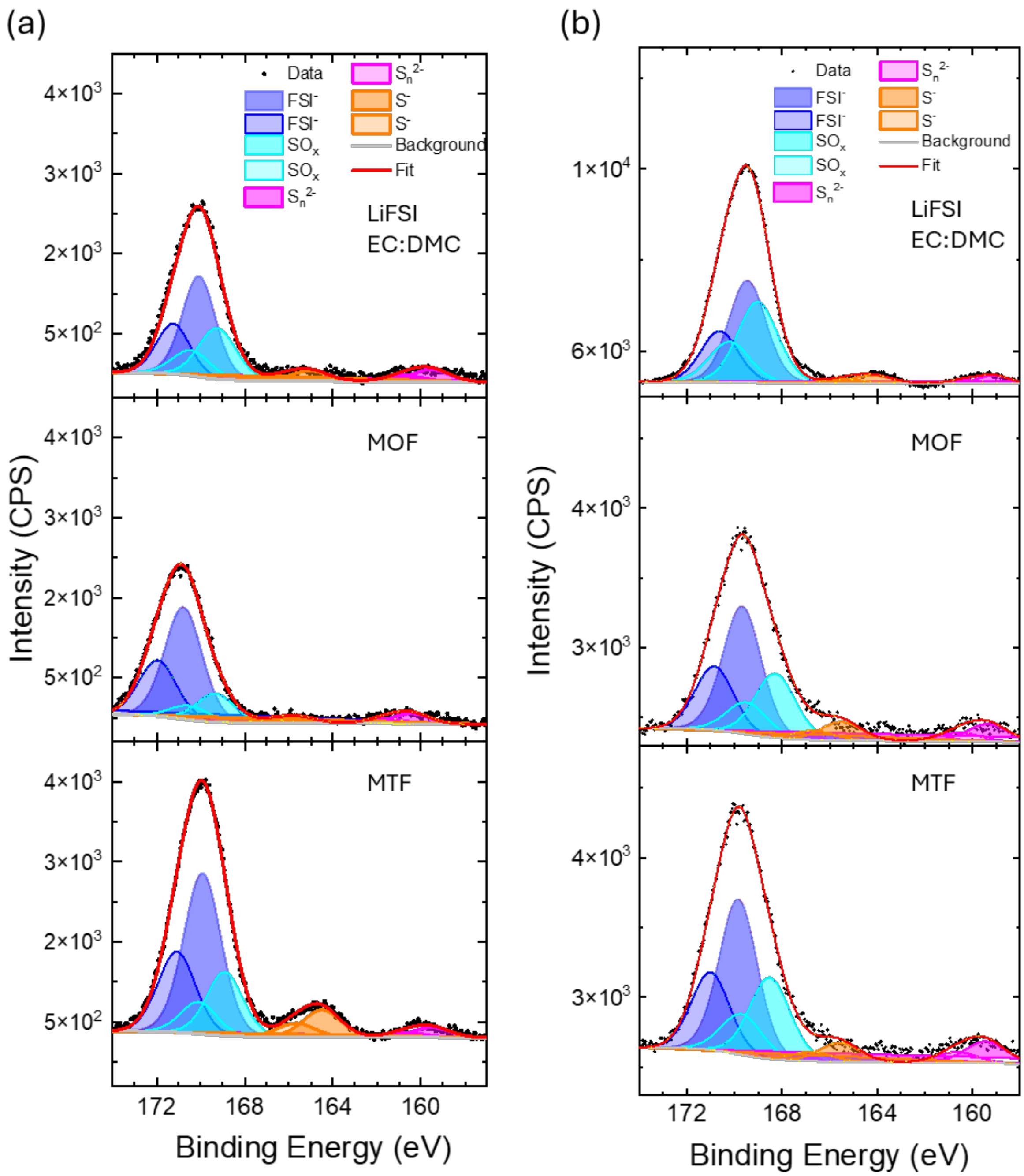

Figure S23. XPS S 2p spectra of recovered (a) NMC811 cathodes and (b) graphite anodes after 200x cycles under the 1C/1C CCCV cycling condition with either LiFSI EC:DMC, MOF, or MTF electrolytes.

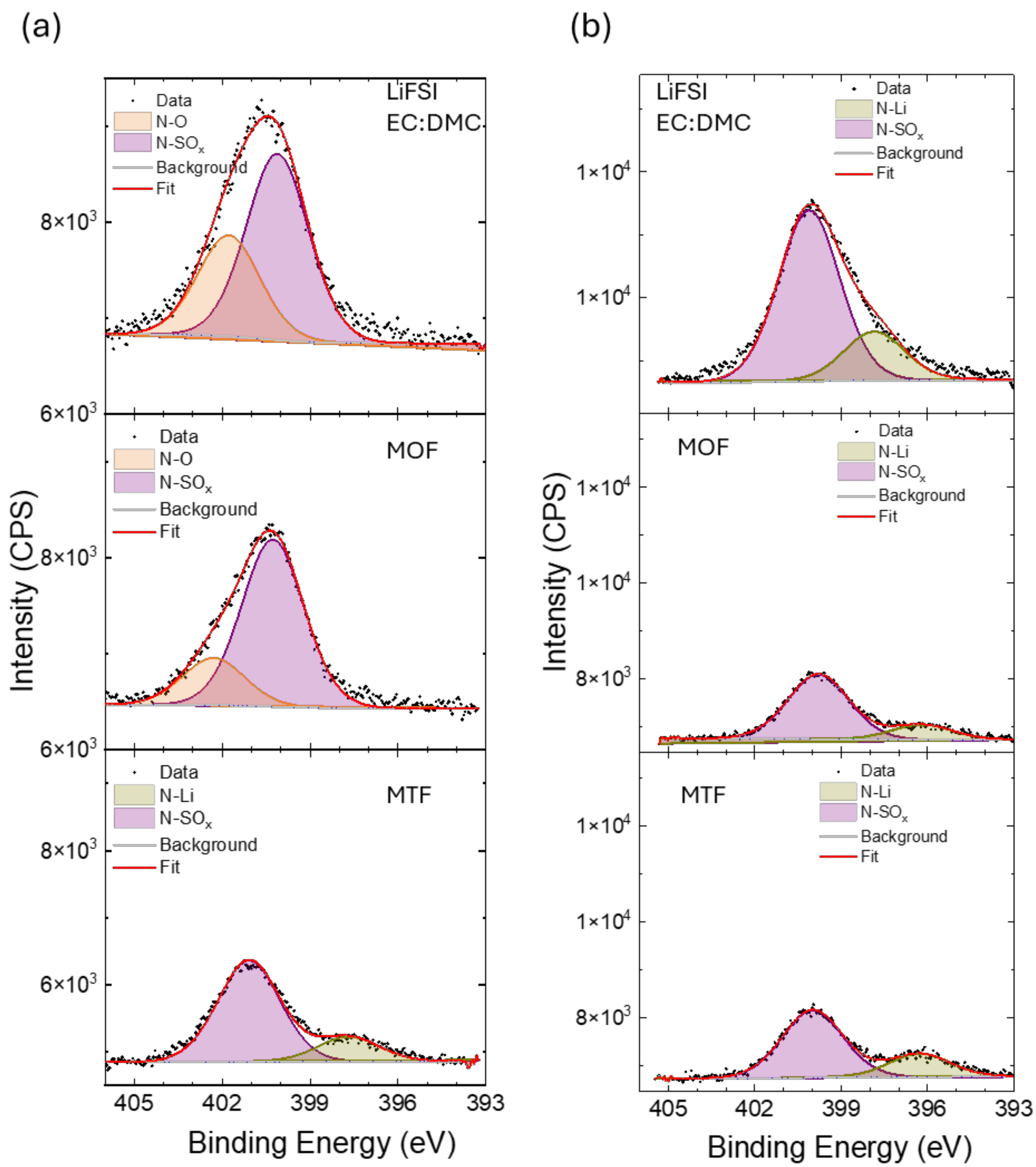

Figure S24. XPS N 1s spectra of recovered (a) NMC811 cathodes and (b) graphite anodes after 200x cycles under the 1C/1C CCCV cycling condition with either LiFSI EC:DMC, MOF, or MTF electrolytes.

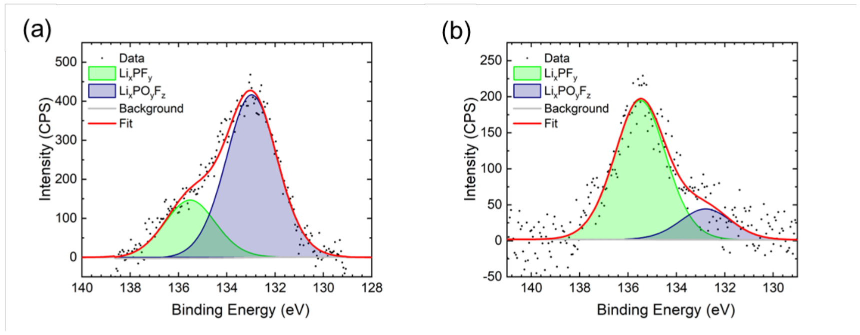

Figure S25. XPS P 2p spectra of recovered (a) NMC811 cathodes and (b) graphite anodes after 200x cycles under the 1C/1C CCCV cycling condition with $LiPF_6$ EC:DMC electrolyte.

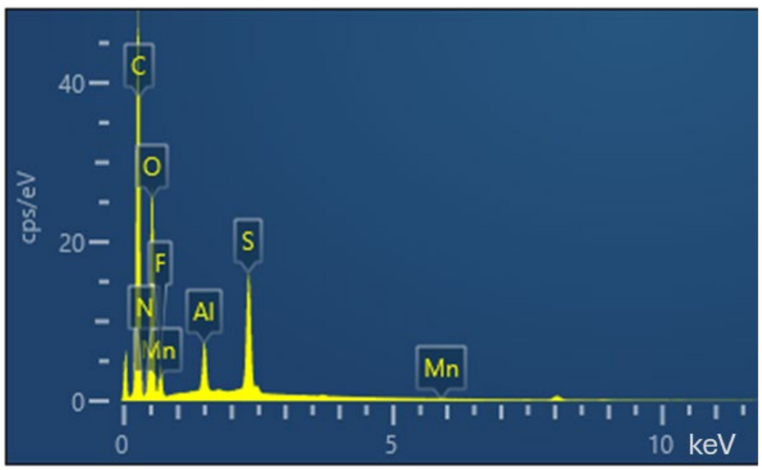

Figure S26. EDS spectra of anode after 200x cycles under the 1C/1C CCCV cycling condition of LiFSI EC:DMC electrolyte.

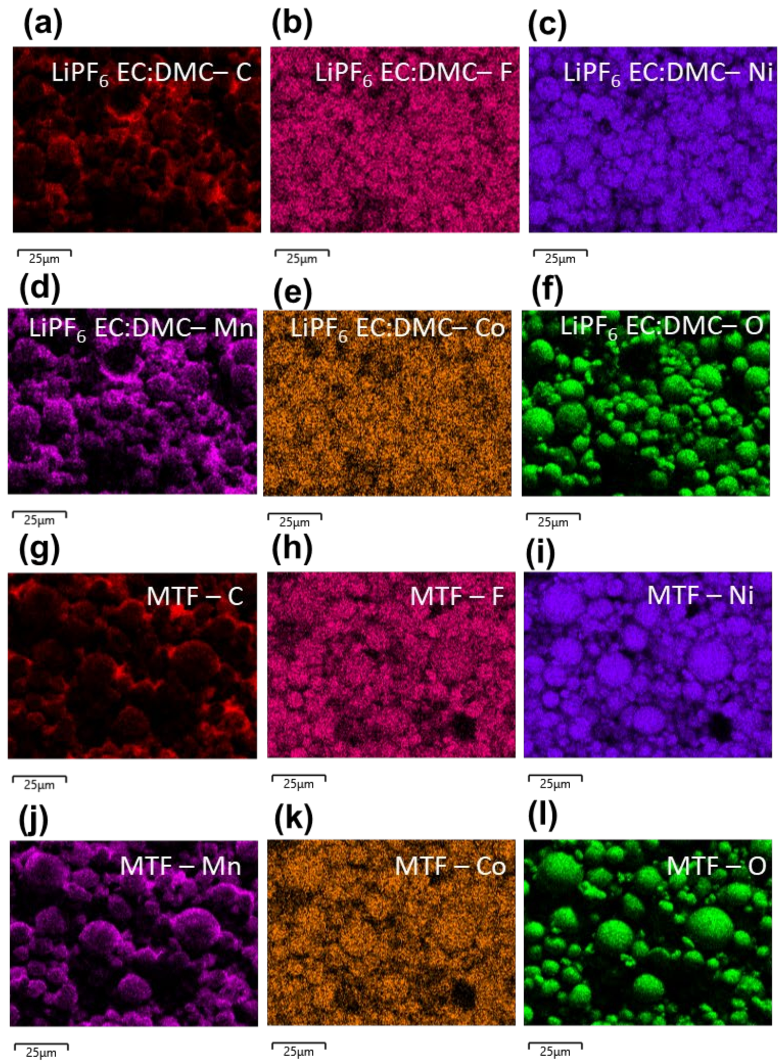

(m)

	$LiPF_6$ EC:DMC (%)	MTF (%)
Ni	11.9	12.9
Mn	1.7	1.7
Co	1.5	1.6
O	23.8	21.6
C	54.5	48.1
F	6.3	13.9
S	0	0.2
Al	0.3	0

Figure S27. (a-l) EDS maps of NMC811 cathodes cycled 200 times under the 1C/1C CCCV condition with either (a-f) $LiPF_6$ EC:DMC or (g-l) MTF electrolyte. (m) Corresponding atomic percentages from the EDS maps.

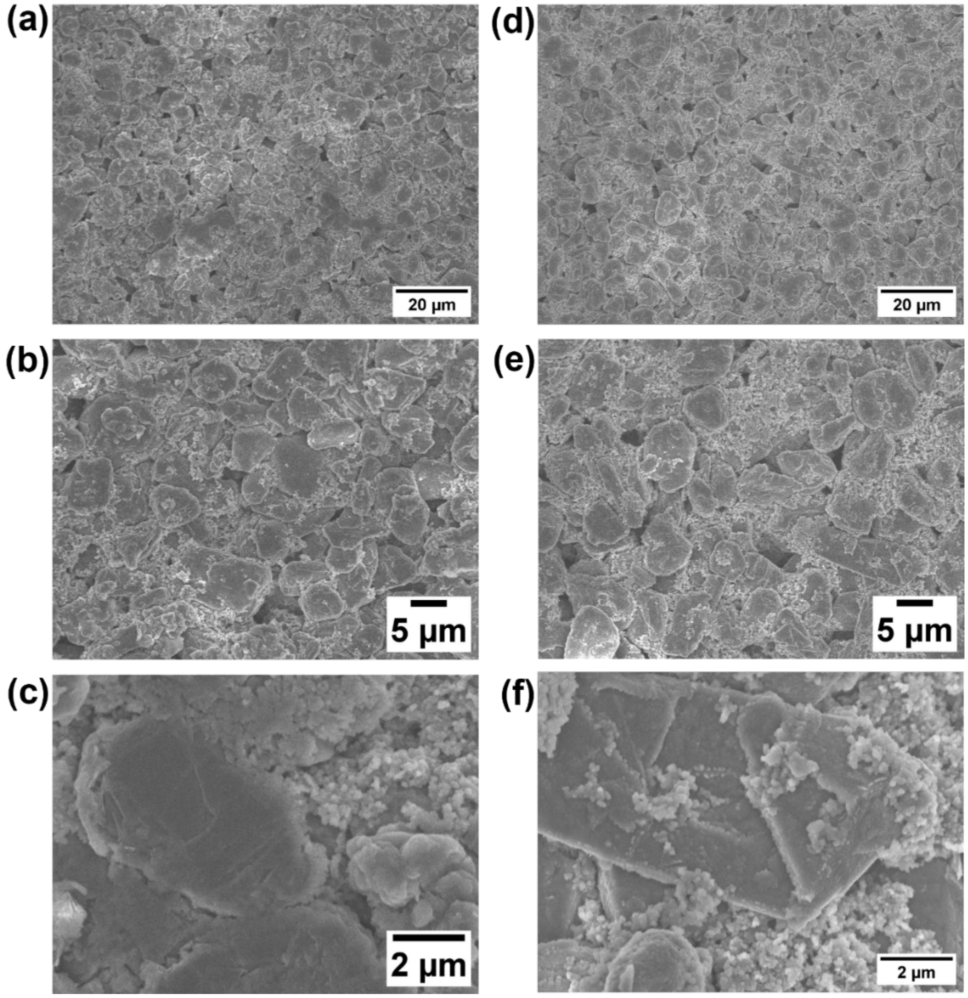

Figure S28. SEM images of graphite anodes cycled 200 times under the 1C/1C CCCV condition. A $LiPF_6$ EC:DMC anode at (a) 1000X, (b) 2000X, and (c) 5000X magnification. An MTF anode at (d) 1000X, (e) 2000X, and (f) 5000X magnification.

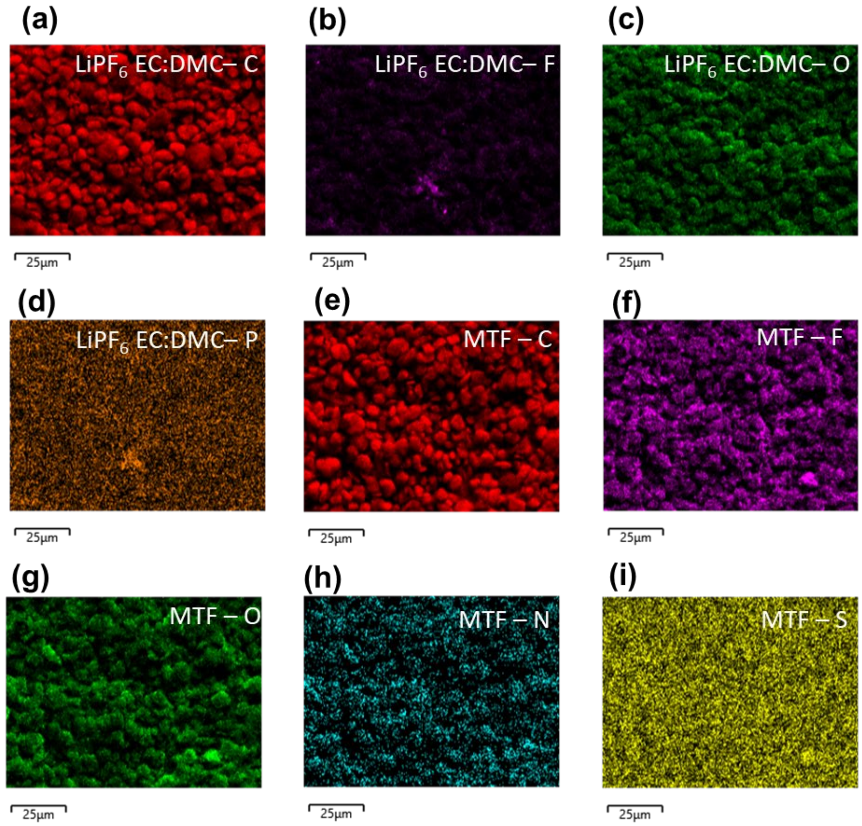

(j)

	$LiPF_6$ EC:DMC (%)	MTF (%)
Ni/Mn/Co	0	0
O	14.0	11.3
C	81.9	78.0
F	4.1	6.9
P	0.1	0
S	0	0.2
N	0	3.6

Figure S29. (a-l) EDS maps of graphite anodes cycled 200 times under the 1C/1C CCCV condition with either (a-f) $LiPF_6$ EC:DMC or (g-l) MTF electrolyte. (m) Corresponding atomic percentages from the EDS maps.

Table S1. Tabulated average 1st cycle irreversible capacities and average 1st and 4th cycle Coulombic efficiencies.

Electrolyte	Irreversible Capacity (mAh/g)	Coulombic Efficiency Cycle 1 (%)	Coulombic Efficiency Cycle 4 (%)
$LiPF_6$ EC:DMC	37	84.3	99.1
LiFSI EC:DMC	38	84.0	99.1
MO LHCE	63	72.8	98.8
MT LHCE	76	67.1	98.5
MOV	41	82.2	99.2
MOF	40	82.7	99.3
MTV	40	82.5	99.1
MTF	38	83.3	99.4

Table S2. Capacity retention of cells under the 1C/1C CCCV and extreme conditions. 1C retention is the 200th 1C discharge capacity divided by the first 1C discharge capacity. C/10 retention is the final C/10 discharge capacity divided by the fourth formation discharge capacity. (At -20 °C, 50 cycles were performed on the controls and MOF electrolytes and only 100 were performed on the MTF electrolyte. Only 100 cycles were performed on the LiFSI EC:DMC at high voltage).

Electrolyte	**Baseline**		**40 °C**		**-20 °C**	
Retention	1C (%)	C/10 (%)	1C (%)	C/10 (%)	1C (%)	C/10 (%)
$LiPF_6$ EC:DMC	78 +/- 2	79 +/- 1	82 +/- 2	83 +/- 2	37 +/- 5	93 +/- 1
LiFSI EC:DMC	48 +/- 1	64 +/- 1	40 +/- 1	50 +/- 2	42 +/- 1	92 +/- 1
MOF	87 +/- 4	90 +/- 2	85 +/- 2	84 +/- 3	61 +/- 3	96 +/- 3
MTF	93 +/- 1	92 +/- 1	80 +/- 3	80 +/- 2	88 +/- 21	93 +/- 1

Electrolyte	**High voltage**		**Fast charge**	
Retention	1C (%)	C/10 (%)	1C (%)	C/10 (%)
$LiPF_6$ EC:DMC	57 +/- 1	66 +/- 1	72 +/- 4	75 +/- 5
LiFSI EC:DMC	0.2 +/- 0.2	18 +/- 18	53 +/- 9	56 +/- 6
MOF	66 +/- 2	76 +/- 2	89 +/- 3	87 +/- 1
MTF	66 +/- 1	73 +/- 1	95 +/- 3	94 +/- 1

Table S3. Conductivities of electrolytes at -20 °C.

Electrolyte	Measured Conductivity (mS/cm)
$LiPF_6$ EC:DMC	1.7 +/- 0.2
LiFSI EC:DMC	2.0 +/- 0.2
MOF	1.1 +/- 0.1
MTF	2.25 +/- 0.04

Table S4. XPS peak assignments for the anodes cycled with FLHCEs

Sample XPS Line	$LiPF_6$ (Control) BE (FWHM) at%	LiFSI (Control) BE (FWHM) at%	LiFSI/MOF BE (FWHM) at%	LiFSI/MTF BE (FWHM) at%	Chemistry
C 1s					
	288.0 (1.7) 0.81	287.9 (1.8) 2.32	287.8 (1.7) 5.84	287.9 (1.8) 5.35	C=O, O-C-O
	286.5 (1.7) 4.83	286.4 (1.8) 7.53	286.3 (1.7) 10.34	286.4 (1.8) 9.55	C-O, C-O-C
	285.0 (1.7) 8.57	284.9 (1.8) 10.58	284.8 (1.7) 14.77	284.9 (1.8) 16.33	C-C, C-H
	290.4 (1.7) 2.98	290.3 (1.8) 1.42	290.3 (1.7) 3.36	290.4 (1.8) 3.08	PVDF, Li_2CO_3
	289.0 (1.7) 1.67	288.9 (1.8) 0.63	288.8 (1.7) 1.77	288.9 (1.8) 1.84	O-C=O
	283.1 (2.5) 2.01		283 (2.5) 1.51	282.4 (1.7) 0.66	C-Li
O 1s					
	528.2 (2.3) 0.87	530.0 (1.9) 0.61	529.4 (3.0) 0.63	529.0 (3.0) 0.7	Li_2O
	531.6 (2.4) 11.03	532.5 (2) 29.11	532.2 (2.3) 14.25	532.4 (2.4) 16.49	C=O, CO_3
	533.6 (2.4) 2.33	534.2 (2) 3.45	533.7 (2.3) 7.3	533.9 (2.4) 6.08	C-O
F 1s					
		686.2 (2.2) 18.07			Me-F
	685.0 (1.9) 20.26	685.0 (2.5) 1.46	684.8 (1.9) 8.78	684.9 (1.9) 5.15	LiF
		688.0 (2.5) 1.83	687.7 (2.2) 8.65	687.8 (2.3) 0.59	FSI^-, PVDF
	687.6 (2.3) 6.86				$Li_xPF_yO_z$, Li_xPF_y, PVDF
Li 1s					
	57.6 (1.9) 1.07	56.6 (1.5) 5.89	56.4 (1.6) 2.76	56.4 (1.6) 4.76	LiF
	55.6 (1.9) 30.83	55.7 (1.5) 6.28	55.4 (1.6) 15.03	55.6 (1.6) 23.47	Li_2CO_3
	53.8 (1.9) 5.06	53.2 (1.5) 0.69	53.8 (1.6) 2.14	53.8 (1.6) 2.46	Li_2O
S 2p					
		169.4 (1.8) 3.35	169.6 (1.9) 1.02	169.8 (1.8) 1.23	$2p_{3/2}$ FSI^-
		170.6 (1.8) 1.67	170.8 (1.9) 0.51	171 (1.8) 0.61	$2p_{1/2}$ FSI^-
		169.0 (2.0) 2.87	168.3 (2.0) 0.54	168.5 (2.0) 0.69	$2p_{3/2}$ SO_x
		170.2 (2.0) 1.43	169.4 (2.0) 0.27	169.7 (2.0) 0.34	$2p_{1/2}$ SO_x
		159.1 (1.5) 0.21	159.3 (2.0) 0.14	159.4 (2.0) 0.18	$2p_{3/2}$ S_2^-
		160.3 (1.5) 0.1	160.5 (2.0) 0.07	160.6 (2.0) 0.09	$2p_{1/2}$ S_2^-
		164.2 (2.0) 0.27	165.5 (2.0) 0.15	165.5 (2.0) 0.16	$2p_{3/2}$ S^-
		165.4 (2.0) 0.13	166.6 (2.0) 0.07	166.7 (2.0) 0.08	$2p_{1/2}$ S^-

Table S4 cont. XPS peak assignments for the anodes cycled with FLHCEs

Sample XPS Line	$LiPF_6$ (Control) BE (FWHM) at%	LiFSI (Control) BE (FWHM) at%	LiFSI/MOF BE (FWHM) at%	LiFSI/MTF BE (FWHM) at%	Chemistry
N 1s					
		400.1 (2.5) 4.45	399.7 (2.5) 2.41	399.9 (2.5) 2.53	$N\text{-}SO_x$
		397.8 (2.5) 1.33	396.1 (2.5) 0.59	396.2 (2.5) 0.92	Li_3N
P 2p					
	136.4 (2.5) 0.19				Li_xPF_y
	133.8 (2.5) 0.54				$Li_xPO_yF_z$

Table S5. XPS peak assignments for the cathodes cycled with FLHCEs

Sample XPS Line	$LiPF_6$ (Control) BE (FWHM) at%	LiFSI (Control) BE (FWHM) at%	LiFSI/MOF BE (FWHM) at%	LiFSI/MTF BE (FWHM) at%	Chemistry
C 1s					
	287.9 (1.6) 2.07	287.9 (1.7) 2.78	287.9 (1.8) 6.41	287.9 (1.8) 4.7	O-C=O, C=O, O-C-O
	286.4 (1.6) 12.78	286.4 (1.7) 10.94	286.4 (1.8) 13.73	286.4 (1.8) 7.82	CH_2, PVDF, C-O
	284.9 (1.6) 28.11	284.9 (1.7) 21.69	284.9 (1.8) 24.52	284.9 (1.8) 13.57	C-C, C-H
	290.5 (1.6) 9.96	290.4 (1.7) 7.03	290.3 (1.8) 7.22	290.2 (1.8) 2.98	PVDF, Li_2CO_3
	288.9 (1.6) 1.83	288.9 (1.7) 1.15	288.9 (1.8) 1.72	288.9 (1.8) 1.3	O-C=O
O 1s					
	529.4 (2.3) 0.47	530.0 (3.0) 0.00	530.0 (2.8) 0.96	530.0 (2.0) 0.38	Li_2O, Me-O
	532.1 (2.5) 9.28	532.0 (2.3) 2.06	532.6 (2.2) 17.42	532.8 (2.3) 17.34	C=O, CO_3
	533.6 (2.5) 2.41	533.9 (2.3) 23.3	534.1 (2.2) 5.18	534.3 (2.3) 3.73	C-O
F 1s					
	687.3 (2.4) 24.9	687.3 (2.5) 22.74	687.6 (2.3) 16.89	687.8 (2.8) 10.9	F-C-F, PVDF
	684.9 (1.9) 2.42	685.2 (1.7) 1.77	684.9 (1.2) 0.77	685.2 (1.9) 11.99	LiF
Li 1s					
	56.6 (2.2) 1.72	56.6 (1.9) 3.29		56.4 (1.7) 15.74	LiF
	55.2 (2.2) 2.84	55.8 (1.9) 1.31	55.8 (1.4) 3.03	55.8 (1.7) 6.38	Li_2CO_3
	52.3 (2.2) 0.41	54 (1.9) 0.77	54.2 (1.4) 0.99	54.4 (1.7) 2.1	Li_2O
S 2p					
		169.9 (2.0) 0.14	170.0 (1.7) 0.14	170.7 (2.0) 0.12	$2p_{3/2}$ FSI^-
		171.0 (2.0) 0.14	171.2 (1.7) 0.14	171.9 (2.0) 0.13	$2p_{1/2}$ FSI^-
		168.9 (1.9) 0.14	169.2 (2.0) 0.14	169.3 (2.0) 0.12	$2p_{3/2}$ SO_x
		170.0 (1.9) 0.14	170.4 (2.0) 0.14	170.5 (2.0) 0.12	$2p_{1/2}$ SO_x
		159.5 (2.0) 0.13	159.5 (2.0) 0.13	160.4 (2.0) 0.12	$2p_{3/2}$ S_2^-
		160.7 (2.0) 0.13	160.7 (2.0) 0.13	161.6 (2.0) 0.12	$2p_{1/2}$ S_2^-
		164.4 (2.0) 0.13	165.0 (2.0) 0.13	165.5 (2.0) 0.12	$2p_{3/2}$ S^-
		165.6 (2.0) 0.14	166.2 (2.0) 0.13	166.7 (2.0) 0.12	$2p_{1/2}$ S^-
N 1s					
		401.7 (2.5) 2.24	402.2 (2.5) 1.03		N-O
		400.1 (2.5) 4.14	400.2 (2.5) 3.66	401.0 (2.5) 2.9	N-SO_x
				397.6 (2.5) 0.75	N-Li

Table S5 cont. XPS peak assignments for the cathodes cycled with FLHCEs

Sample XPS Line	$LiPF_6$ (Control) BE (FWHM) at%	LiFSI (Control) BE (FWHM) at%	LiFSI/MOF BE (FWHM) at%	LiFSI/MTF BE (FWHM) at%	Chemistry
P 2p					
	136.2 (2.3) 0.59				Li_xPF_y
	133.7 (2.5) 0.13				$Li_xPO_yF_z$

Table S6. Comparison of this work and previous works on LHCE cycling with an emphasis on cycling under multiple extreme conditions. (n.s.=not stated, n.t.=not tested, N.F.=nonflammable, flam.=flammability, NMC=$LiNi_xMn_yCo_zO_2$, LFP=$LiFePO_4$, NC9406=$LiNi_{0.94}Co_{0.06}O_2$).

Cathode, loading (mAh/cm^2)	Anode, loading (mAh/cm^2)	Electrolyte	Conductivity at 25 °C	Cell Type	Ref.
NMC811, 1.7	**Graphite, 2**	**LiFSI in MTFP-TFETFE-FEC**	**7.0**	**Pouch**	**This work**
NMC811, 1.5	Graphite, 2	1.2 M LiFSI/TEPa-EC-BTFE	1.3 mS/cm	Coin	[16]
NMC811, 2.8	Graphite, 3.5	1.4 M LiFSI in DMC-EC-TTE	1.0 mS/cm	Coin	[17]
Li-rich NMC, 1.34	Graphite, 1.8	1.4 M LiFSI in DMC-EC-TTE	n.t.	Coin	[18]
LFP, 1.5	Graphite, 1.8	LiFSI in TMP_a-EC-TTFEP	0.8 mS/cm	Coin	[19]
NMC811, 1.5	Graphite, 1.8	1.9 M LiFSI in TFE TFMS/TFE MS	n.t.	Pouch	[20]
NMC811, 2.5	Graphite, 2.7	1 M LiTFSI MDFA/MDFSA-TTE	1.7 mS/cm	Pouch	[21]
NMC111, 1.93	Silicon-graphite, 2.2	1.2 M LiFSI in TEP/FEC/BTFE	1.3 mS/cm	Coin	[22]
NMC532, 2.0	Silicon-graphite, 3	LiFSI in EC/EMC/BTFE	0.68-1.96 mS/cm	Coin	[23]
NMC811, 4.2	Lithium, 50 µm	LiFSI in DME/TFEO	1.43-5.65 mS/cm	Coin	[24]
NMC111, 2.0	Lithium, 450 µm	1.2 M LiFSI in DMC/BTFE	1.80-2.67 mS/cm	Coin	[25]
NMC622, 1.6	Lithium, 450 µm	1.2 M LiFSI in TEP/BTFE	1.29 mS/cm	Coin	[26]
NMC811, 1.5	Lithium, 250 µm	LiFSI-TMS/TTE	2.03 mS/cm	Coin	[27]
NMC811, 1.5/4.2	Lithium, 450 µm	LiFSI-DME-TTE	2.44 mS/cm	Coin	[28]
NMC333, 1	Lithium, 250 µm	1.2 M LiFSI in EC/EMC/BTFE/LiDFOB	n.t.	Coin	[29]
NC9406, 2.0	Lithium, n.s.	LiPF6-EC-EMC/ LiFSI-DME-TTE	n.t.	Pouch	[30]
NMC811, 3.3	Lithium, n.s	LiFSI-DPE, DEE, DME, DIG	0.6-11 mS/cm	Coin	[31]
NMC811, 4	Lithium, 50 µm	LiPF6-EC/DEC +FEC+LiDFOB	n.t.	Pouch	[32]
NMC811, 3.5	Lithium, 20 µm	LiFSI in DME-TFMB or BZTF	1.6-3.5 mS/cm	Pouch	[33]
NC9406, 1.6	Lithium, 250 µm	LiFSI in DME-TTE	n.t.	Pouch	[34]
$LiCoO_2$, 0.6	Lithium, n.s.	(1, 2, n) M LiFSA/SL/HFE (n= 0, 0.5, 1, 2)	1.9-2.2 mS/cm	Coin	[35]
NMC622, 4	Lithium, 25 µm	1.5 M LiFSI DME/PFPN 1:2	2.5-7.5 mS/cm	Coin	[36]
NMC622, 1.5	Lithium, n.s.	LiFSI in DME-TTE	2-10 mS/cm	Coin	[37]
NMC532, 0.5	Lithium, 1 mm	LDFP/G4/HFE/FEC	0.04-0.045 mS/cm	Coin	[38]
NMC811, n.s.	Lithium, 500 µm	2.3 M LiFSI/TEP/FB	0.83-0.93 mS/cm	Coin	[39]
NMC811, 4	Lithium, 50 µm	LiFSI in FEC-DME-TTE + LiDFOB	n.t.	Coin	[40]

Baseline	High Temperature (≥40 °C)	Low Temperature (≤0 °C)	High Charge Voltage (≥4.5 V)	Fast Charge Rate (≥4C)	Flam.	Ref
Charge rate, voltage window, initial capacity, retention, cycle #	**Charge rate, voltage window, initial capacity, retention, cycle #, T**	**Charge rate, voltage window, initial capacity, retention, cycle #, T**	**Charge rate, voltage window, initial capacity, retention, cycle #**	**Charge rate, voltage window, initial capacity, retention, cycle #**		
1C, 3-4.3 V, 180 mAh/g, 93%, 200	1C, 3-4.3 V, 184 mAh/g, 80%, 200, 40 °C	1C, 3-4.3 V, 107 mAh/g, 88%, 100, -20 °C	1C, 3-4.5 V, 184 mAh/g, 66%, 200	4C, 3-4.3 V, 178 mAh/g, 95%, 200	N.F.	**This work**
C/2, 2.8-4.3 V, 160 mAh/g, 85%, 300	n.t.	n.t.	n.t.	n.t.	N.F.	[16]
C/3, 2.5-4.4 V, 173 mAh/g, 94.2%, 600	C/3, 2.5-4.4 V, 183.6 mAh/g, 94.9%, 100	C/5, 2.5-4.4 V, 175, 160, and 80 mAh/g at -20, -30, -40 °C for one cycle	n.t.	5C, 2.5-4.4 V, 30 mAh/g for 5 cycles	n.t.	[17]
n.t.	C/3, 2.7-4.7 V, 230 mAh/g, 54.0%, 100, 60 °C	n.t.	C/3, 2.7-4.7 V, 195 mAh/g, 91.7%, 100	n.t.	n.t.	[18]
C/5, 2.8-3.9 V, 115 mAh/g, 80%, 300	n.t.	n.t.	n.t.	n.t.	N.F.	[19]
n.t.	1C, 2.8-4.6 V, 190 mAh/g, 80%, 190, 60 °C	n.t.	1C, 2.8-4.6 V, 200 mAh/g, 85%, 2000	n.t.	N.F.	[20]
n.t.	C/2, 2.5-4.5 V, 220 mAh/g, 73.1%, 180, 60 °C	C/5, 2.5-4.5 V, 160 mAh/g, 82.8%, 360, -30 °C	C/2, 2.5-4.5 V, 220 mAh/g, 80.1%, 400	4C, 2.5-4.5 V, 150 mAh/g, 87%, 300	N.F.	[21]
C/6, 2.7-4.2 V, 140 mAh/g, 89.8%, 600	C/6, 2.7-4.2 V, 140 mAh/g, 90.2%, 200, 45 °C	n.t.	n.t.	n.t.	N.F.	[22]
C/3, 3-4.1 V, 118 mAh/g, 81.8%, 200	n.t.	n.t.	C/3, 3-4.5 V, 175 mAh/g, 92.7%, 60	n.t.	n.t.	[23]
C/10, 2.8-4.4 V, 200 mAh/g, 80%, 200	n.t.	n.t.	n.t.	n.t.	n.t.	[24]
C/2, 2.7-4.3 V, 150 mAh/g, 80%, 700	n.t.	n.t.	n.t.	n.t.	n.t.	[25]
C/3, 2.8-4.4 V, 175 mAh/g, 97%, 600	n.t.	n.t.	n.t.	n.t.	N.F.	[26]
C/3, 2.7-4.3 V, 160 mAh/g, 88%, 300	n.t.	C/3, 2.7-4.3 V, 110 mAh/g, 22 cycles, -10 °C	1C, 3.2-4.9 V, 95 mAh/g, 95%, 100 (LNMO, 3 mg/cm^2)	n.t.	n.t.	[27]

C/3, 2.8-4.4 V, 205 mAh/g, 87%, 300	n.t.	n.t.	C/3, 2.8-4.5 V, 210 mAh/g, 82%, 250	140 mAh/g for 5 cycles at 4C, 115 mAh/g for 5 cycles at 6C	n.t.	[28]
1C, 2.7-4.3 V, 150 mAh/g, 80%, 400	n.t.	n.t.	n.t.	n.t.	n.t.	[29]
C/2, 3-4.4 V, 210 mAh/g, 89%, 200	n.t.	n.t.	n.t.	n.t.	N.F.	[30]
C/3, 2.5-4.3 V, 180 mAh/g, 80%, 210	C/3, 2.5-4.3 V, 210 mAh/g for 15 cycles at 50 °C	C/20, 2.5-4.3 V, 120 mAh/g for 15 cycles at -40 °C	n.t.	n.t.	n.t.	[31]
C/5, 2.8-4.3 V, 210 mAh/g, 80%, 335	C/5, 2.8-4.3 V, 210 mAh/g, 86%, 100, 60 °C	n.t.	n.t.	n.t.	N.F.	[32]
C/5, 2.8-4.3 V, 205 mAh/g, 80%, 260	n.t.	n.t.	n.t.	205 mAh/g for 5 cycles at 4C, 175 mAh/g for 5 cycles at 10C	n.t.	[33]
C/3, 2.8-4.4 V, 233 mAh/g, 84%, 200	n.t.	n.t.	n.t.	n.t.	n.t.	[34]
C/10, 3-4.2 V, 140 mAh/g, no cycling	n.t.	n.t.	n.t.	n.t.	n.t.	[35]
C/5, 3-4.4 V, 200 mAh/g, 90.7%, 200	C/5, 3-4.4 V, 200 mAh/g, 73.8%, 200, 50 °C	n.t.	C/5, 3-4.5 V, 210 mAh/g, 80%, 170	n.t.	N.F.	[36]
n.t.	n.t.	n.t.	n.t.	12C, 3-4.2 V, 87 mAh/g, 67%, 125	n.t.	[37]
n.t.	C/2, 2.75-4.3 V, 180 mAh/g, 91.4%, 200, 60 °C	C/10, 2.75-4.3 V, 130, 80, 70 mAh/g at -40, -50, -60 °C for one cycle	C/2, 3-4.5 V, 170 mAh/g, 98.5%, 150	n.t.	n.t.	[38]
C/2, 2.8-4.3 V, 180 mAh/g, 86.4%, 500	n.t.	n.t.	n.t.	5C, 2.8-4.3 V, 86 mAh/g for 5 cycles	N.F.	[39]
C/2, 2.7-4.3 V, 200 mAh/g, 80%, 200	n.t.	n.t.	n.t.	n.t.	n.t.	[40]

References

1. J. L. White, F. S. Gittleson, M. Homer and F. El Gabaly, *The Journal of Physical Chemistry C*, 2020, **124**, 16508-16514.

2. K. R. Tallman, G. P. Wheeler, C. J. Kern, E. Stavitski, X. Tong, K. J. Takeuchi, A. C. Marschilok, D. C. Bock and E. S. Takeuchi, *The Journal of Physical Chemistry C*, 2021, **125**, 58-73.

3. D. Briggs and G. Beamson, *Analytical Chemistry*, 1992, **64**, 1729-1736.

4. S. Leroy, F. Blanchard, R. Dedryvere, H. Martinez, B. Carre, D. Lemordant and D. Gonbeau, *Surface and Interface Analysis* 2005, **37**, 773-781.

5. J. F. Moulder, Stickle, W. F., Sobol, P. E. and Bomben, K. D., *Handbook of X-ray Photoelectron Spectroscopy*, ULVAC-PHI, 1995.

6. S.-K. Otto, Y. Moryson, T. Krauskopf, K. Peppler, J. Sann, J. Janek and A. Henss, *Chemistry of Materials*, 2021, **33**, 859-867.

7. D. J. Xiong, L. D. Ellis, J. Li, H. Li, T. Hynes, J. P. Allen, J. Xia, D. S. Hall, I. G. Hill and J. R. Dahn, *Journal of The Electrochemical Society*, 2017, **164**, A3025.

8. K. P. C. Yao, D. G. Kwabi, R. A. Quinlan, A. N. Mansour, A. Grimaud, Y.-L. Lee, Y.-C. Lu and Y. Shao-Horn, *Journal of The Electrochemical Society*, 2013, **160**, A824.

9. M. Hekmatfar, A. Kazzazi, G. G. Eshetu, I. Hasa and S. Passerini, *ACS Applied Materials & Interfaces*, 2019, **11**, 43166-43179.

10. S. Marchesini, B. P. Reed, H. Jones, L. Matjacic, T. E. Rosser, Y. Zhou, B. Brennan, M. Tiddia, R. Jervis, M. J. Loveridge, R. Raccichini, J. Park, A. J. Wain, G. Hinds, I. S. Gilmore, A. G. Shard and A. J. Pollard, *ACS Applied Materials & Interfaces*, 2022, **14**, 52779-52793.

11. D. Andre, M. Meiler, K. Steiner, C. Wimmer, T. Soczka-Guth and D. U. Sauer, *Journal of Power Sources*, 2011, **196**, 5334-5341.

12. M. D. Levi, K. Gamolsky, D. Aurbach, U. Heider and R. Oesten, *Electrochimica Acta*, 2000, **45**, 1781-1789.

13. W. Choi, H.-C. Shin, J. M. Kim, J.-Y. Choi and W.-S. Yoon, *J. Electrochem. Sci. Technol*, 2020, **11**, 1-13.

14. D. Aurbach, M. D. Levi, E. Levi, H. Teller, B. Markovsky, G. Salitra, U. Heider and L. Heider, *Journal of The Electrochemical Society*, 1998, **145**, 3024-3034.

15. A. V. Ivanishchev, A. V. Churikov, I. A. Ivanishcheva, K. V. Zapsis and I. M. Gamayunova, *Russian Journal of Electrochemistry*, 2008, **44**, 510-524.

16. X. Cao, Y. Xu, L. Zhang, M. H. Engelhard, L. Zhong, X. Ren, H. Jia, B. Liu, C. Niu, B. E. Matthews, H. Wu, B. W. Arey, C. Wang, J.-G. Zhang and W. Xu, *ACS Energy Letters*, 2019, **4**, 2529-2534.

17. X. Zhang, L. Zou, Y. Xu, X. Cao, M. H. Engelhard, B. E. Matthews, L. Zhong, H. Wu, H. Jia, X. Ren, P. Gao, Z. Chen, Y. Qin, C. Kompella, B. W. Arey, J. Li, D. Wang, C. Wang, J.-G. Zhang and W. Xu, *Advanced Energy Materials*, 2020, **10**, 2000368.

18. X. Zhang, H. Jia, Y. Xu, L. Zou, M. H. Engelhard, B. E. Matthews, C. Wang, J.-G. Zhang and W. Xu, *Journal of Power Sources Advances*, 2020, **5**, 100024.

19. H. Jia, Z. Yang, Y. Xu, P. Gao, L. Zhong, D. J. Kautz, D. Wu, B. Fliegler, M. H. Engelhard, B. E. Matthews, B. Broekhuis, X. Cao, J. Fan, C. Wang, F. Lin and W. Xu, *Advanced Energy Materials*, 2023, **13**, 2203144.

20. J. Zhang, H. Zhang, S. Weng, R. Li, D. Lu, T. Deng, S. Zhang, L. Lv, J. Qi, X. Xiao, L. Fan, S. Geng, F. Wang, L. Chen, M. Noked, X. Wang and X. Fan, *Nature Communications*, 2023, **14**, 2211.

21. J. Xu, J. Zhang, T. P. Pollard, Q. Li, S. Tan, S. Hou, H. Wan, F. Chen, H. He, E. Hu, K. Xu, X.-Q. Yang, O. Borodin and C. Wang, *Nature*, 2023, **614**, 694-700.

22. H. Jia, L. Zou, P. Gao, X. Cao, W. Zhao, Y. He, M. H. Engelhard, S. D. Burton, H. Wang, X. Ren, Q. Li, R. Yi, X. Zhang, C. Wang, Z. Xu, X. Li, J.-G. Zhang and W. Xu, *Adv. Energy Mater.*, 2019, **9**, n/a.

23. H. Jia, P. Gao, L. Zou, K. S. Han, M. H. Engelhard, Y. He, X. Zhang, W. Zhao, R. Yi, H. Wang, C. Wang, X. Li and J.-G. Zhang, *Chemistry of Materials*, 2020, **32**, 8956-8964.

24. X. Cao, L. Zou, B. E. Matthews, L. Zhang, X. He, X. Ren, M. H. Engelhard, S. D. Burton, P. Z. El-Khoury, H.-S. Lim, C. Niu, H. Lee, C. Wang, B. W. Arey, C. Wang, J. Xiao, J. Liu, W. Xu and J.-G. Zhang, *Energy Storage Materials*, 2021, **34**, 76-84.

25. S. Chen, J. Zheng, D. Mei, K. S. Han, M. H. Engelhard, W. Zhao, W. Xu, J. Liu and J.-G. Zhang, *Advanced Materials*, 2018, **30**, 1706102.

26. S. Chen, J. Zheng, L. Yu, X. Ren, M. H. Engelhard, C. Niu, H. Lee, W. Xu, J. Xiao, J. Liu and J.-G. Zhang, *Joule*, 2018, **2**, 1548-1558.

27. X. Ren, S. Chen, H. Lee, D. Mei, M. H. Engelhard, S. D. Burton, W. Zhao, J. Zheng, Q. Li, M. S. Ding, M. Schroeder, J. Alvarado, K. Xu, Y. S. Meng, J. Liu, J.-G. Zhang and W. Xu, *Chem*, 2018, **4**, 1877-1892.

28. X. Ren, L. Zou, X. Cao, M. H. Engelhard, W. Liu, S. D. Burton, H. Lee, C. Niu, B. E. Matthews, Z. Zhu, C. Wang, B. W. Arey, J. Xiao, J. Liu, J.-G. Zhang and W. Xu, *Joule*, 2019, **3**, 1662-1676.

29. L. Yu, S. Chen, H. Lee, L. Zhang, M. H. Engelhard, Q. Li, S. Jiao, J. Liu, W. Xu and J.-G. Zhang, *ACS Energy Letters*, 2018, **3**, 2059-2067.

30. J. Langdon, R. Sim and A. Manthiram, *ACS Energy Letters*, 2022, **7**, 2634-2640.

31. Z. Li, H. Rao, R. Atwi, B. M. Sivakumar, B. Gwalani, S. Gray, K. S. Han, T. A. Everett, T. A. Ajantiwalay, V. Murugesan, N. N. Rajput and V. G. Pol, *Nature Communications*, 2023, **14**, 868.

32. G.-X. Li, H. Jiang, R. Kou, D. Wang, A. Nguyen, M. Liao, P. Shi, A. Silver and D. Wang, *ACS Energy Letters*, 2022, **7**, 2282-2288.

33. C. Zhu, C. Sun, R. Li, S. Weng, L. Fan, X. Wang, L. Chen, M. Noked and X. Fan, *ACS Energy Letters*, 2022, **7**, 1338-1347.

34. J. Langdon and A. Manthiram, *Advanced Materials*, 2022, **34**, 2205188.

35. Y. Watanabe, Y. Ugata, K. Ueno, M. Watanabe and K. Dokko, *Physical Chemistry Chemical Physics*, 2023, **25**, 3092-3099.

36. Q. Liu, Y. Liu, Z. Chen, Q. Ma, Y. Hong, J. Wang, Y. Xu, W. Zhao, Z. Hu, X. Hong, J. Wang, X. Fan and H. B. Wu, *Advanced Functional Materials*, 2023, **33**, 2209725.

37. M. A. Baird, J. Song, R. Tao, Y. Ko and B. A. Helms, *ACS Energy Letters*, 2022, **7**, 3826-3834.

38. S. Kuang, H. Hua, P. Lai, J. Li, X. Deng, Y. Yang and J. Zhao, *ACS Applied Materials & Interfaces*, 2022, **14**, 19056-19066.

39. Z. Xu, K. Deng, S. Zhou, Z. Liu, X. Guan and D. Mo, *ACS Applied Materials & Interfaces*, 2022, **14**, 48694-48704.

40. F. Guo, X. Chen, Y. Hou, W. Wei, Z. Wang, H. Yu and J. Xu, *Small*, 2023, **19**, 2207290.